



HAL
open science

Numerical analysis of the Factorization Method for Electrical Impedance Tomography in inhomogeneous medium

Housseem Haddar, Giovanni Migliorati

► **To cite this version:**

Housseem Haddar, Giovanni Migliorati. Numerical analysis of the Factorization Method for Electrical Impedance Tomography in inhomogeneous medium. [Research Report] RR-7801, 2011, pp.34. hal-00641260v1

HAL Id: hal-00641260

<https://inria.hal.science/hal-00641260v1>

Submitted on 15 Nov 2011 (v1), last revised 24 Jul 2013 (v2)

HAL is a multi-disciplinary open access archive for the deposit and dissemination of scientific research documents, whether they are published or not. The documents may come from teaching and research institutions in France or abroad, or from public or private research centers.

L'archive ouverte pluridisciplinaire **HAL**, est destinée au dépôt et à la diffusion de documents scientifiques de niveau recherche, publiés ou non, émanant des établissements d'enseignement et de recherche français ou étrangers, des laboratoires publics ou privés.

***Numerical analysis of the Factorization Method for
Electrical Impedance Tomography in
inhomogeneous medium***

Housseem Haddar — Giovanni Migliorati

N° 7801

October 2011

Thème NUM



***rapport
de recherche***

Numerical analysis of the Factorization Method for Electrical Impedance Tomography in inhomogeneous medium

Housseem Haddar*, Giovanni Migliorati†

Thème NUM — Systèmes numériques
Équipes-Projets DeFI

Rapport de recherche n° 7801 — October 2011 — 33 pages

Abstract: The retrieval of informations on the coefficient in Electrical Impedance Tomography is a severely ill-posed problem, and often leads to inaccurate solutions. It is well-known that numerical methods provide only low-resolution reconstructions. The aim of this work is to analyze the Factorization Method in the case of inhomogeneous background. We propose a numerical scheme to solve the dipole-like Neumann boundary-value problem, when the background coefficient is inhomogeneous. Several numerical tests show that the method is capable of recovering the location and the shape of the inclusions, in many cases where the diffusion coefficient is nonlinearly space-dependent. In addition, we test the numerical scheme after adding artificial noise.

Key-words: Inverse Problems, Factorization Method, Electrical Impedance Tomography

* INRIA Saclay Ile de France and Ecole Polytechnique (CMAP)

† Dipartimento di Matematica “Francesco Brioschi”, Politecnico di Milano and Ecole Polytechnique (CMAP)

Rapport de Recherche

Inria

Résumé : Nous nous intéressons dans ce travail à l'application de la méthode de Factorization à l'imagerie par impédance électrique dans des milieux hétérogènes. Nous proposons un schéma numérique qui se base sur une évaluation précise de la fonction de Green du milieu. Plusieurs tests numériques sont effectués démontrant de bonnes performances de la méthode, très comparables au cas de milieux homogènes.

Mots-clés : Problèmes inverses, la méthode de factorisation, tomographie d'impédance électrique

1 Introduction

The problem of *Electrical Impedance Tomography* (EIT) arises in many applied contexts. It leads to well established operative procedures, *e.g.* in geophysics, nondestructive testing or imaging applications, while in other fields its usage is still experimental *e.g.* medicine, [4] [13] [18].

The rigorous framework of the EIT problem was set up for the first time by Calderón in his seminal paper [8]. Briefly, it concerns the determination of the coefficient of a given (elliptic) PDE model from the (complete or incomplete) knowledge of suitable maps, *e.g.* the *Dirichlet-to-Neumann map* (DtNm).

In the isotropic case, the uniqueness of the solution to the two-dimensional conductivity inverse problem has been showed in the general L^∞ case in [3]. In three dimensions the uniqueness is proved if additional smoothness on the coefficient is assumed [5]. Concerning stability, at the moment there exist only logarithmic-type estimates in two dimensions (and higher) [1]. The anisotropic case is much less complete. In general, even the complete knowledge of the DtNm does not allow to uniquely recover the coefficient, but some partial answers are present in the literature [16].

Many mathematical models for EIT were proposed, trying to take into account as many physical phenomena as possible. In this work we address the Factorization Method (see [14]) applied to the *Continuous Model* (CM) in the context of EIT featuring an inhomogeneous isotropic background. The aim is to recover the support of unknown inclusions from the knowledge of indirect boundary measurements. We propose a numerical scheme to solve the dipole-like Neumann boundary-value problem, when the background coefficient is inhomogeneous. We treat different types of nonlinearities in the coefficient, and show through several numerical tests that the method is capable of recovering the location and the shape of the inclusions. Moreover, we investigate the robustness of the method applying a random perturbation to the measurement operator. We exhibit the better accuracy of Tychonov regularization with Morozov principle, compared to the simple truncated Picard criterion, which is commonly used in the literature.

1.1 Mathematical formulation

Consider a bounded domain $B \subset \mathbb{R}^2$ and its subset $D \subset B$. We assume that B is a C^2 -domain, but could be Lipschitzian also. Moreover, we assume that D is a union of possibly disjoint Lipschitzian domains, each one with positive measure, and that $B \setminus \overline{D}$ is connected.

The domain B represents the background medium, featured by the physical coefficient σ_B . The domain D represents an obstacle, displaced somewhere inside B , but not too close to the boundary ∂B . The obstacle is characterized by unknown shape and unknown value of its physical coefficient σ_D .

In the last decades a lot of efforts have been dedicated to the research of the minimal regularity assumptions for the coefficients σ_B, σ_D , in order for the EIT problem to be well-posed.

The theory behind EIT does not present any substantial differences between the cases of homogeneous and inhomogeneous background. However, the inhomogeneous background case is numerically much less investigated.

We will consider only homogeneous obstacles, since our main target is the inhomogeneity in the background. The next assumption recaps the case we will focus on, including some technical requirements.

Assumption 1. Assume σ_B is α -Holderian in B with $\alpha > 1$. Moreover, denoting by

$$\sigma_B^m = \min_{x \in B} \sigma_B(x) \quad \text{and} \quad \sigma_B^M = \max_{x \in B} \sigma_B(x),$$

then σ_B and σ_D satisfy

$$0 < \sigma_D < \sigma_B^m < \sigma_B^M < \infty, \quad \text{or} \quad 0 < \sigma_B^m < \sigma_B^M < \sigma_D < \infty.$$

Remark 1. In our numerical scheme the requirement that σ_B is α -Holderian in B can be easily extended to $\sigma_B \in L^\infty(B)$, choosing the sampling points such that they do not fall exactly where σ_B jumps.

Now consider the coefficient $\sigma(x) \in L^\infty(B)$ defined as

$$\sigma(\mathbf{x}) = \begin{cases} \sigma_B(\mathbf{x}), & \text{in } B \setminus D, \\ \sigma_D(\mathbf{x}), & \text{in } D, \end{cases} \quad (1.1)$$

and define the functional spaces

$$\begin{aligned} \dot{L}^2(\partial B) &= \left\{ g \in L^2(\partial B), \int_{\partial B} g = 0 \right\}, & \dot{H}^1(B) &= \left\{ g \in H^1(B), \int_{\partial B} g = 0 \right\}, \\ \dot{H}^{\frac{1}{2}}(\partial B) &= \left\{ g \in H^{\frac{1}{2}}(\partial B), \int_{\partial B} g = 0 \right\}, & \dot{H}^{-\frac{1}{2}}(\partial B) &= \left\{ g \in H^{-\frac{1}{2}}(\partial B), {}_{H^{-1/2}}\langle g, 1 \rangle_{H^{1/2}} = 0 \right\}. \end{aligned}$$

Given $g \in \dot{H}^{-\frac{1}{2}}(\partial B)$, consider the elliptic Neumann boundary-value problem

$$\begin{cases} \nabla \cdot (\sigma(\mathbf{x})\nabla u) = 0, & \text{in } B, \\ \frac{\partial u}{\partial \nu} = g, & \text{on } \partial B. \end{cases} \quad (1.2)$$

The existence of a family of solutions is ensured from Theorem 10 when the function g satisfies the usual compatibility condition and the coefficient σ defined in (1.1) satisfies Assumption 1. To uniquely select a solution we pick the one with null mean on the boundary ∂B .

Proposition 1. Under Assumption 1, it holds $\sigma \in L^\infty(B)$, and for every $g \in \dot{H}^{-\frac{1}{2}}(\partial B)$ there exist a unique solution $u \in \dot{H}^1(B)$ that solves problem (1.2).

In the EIT problem we prescribe a current pattern g and we measure the generated potential $f = u|_{\partial B}$ on the boundary ∂B . The final aim is to retrieve some informations about D , e.g. its location inside B and its shape.

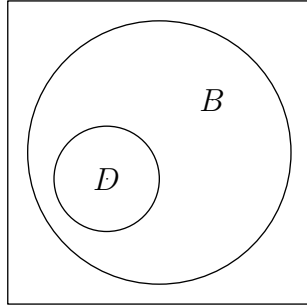


Fig. 1: An obstacle D which lies in a medium B .

The operator Λ that maps currents g into potentials f is the *NtDm* associated to problem (1.2) with coefficient (1.1). It is a continuous operator from $\dot{H}^{-\frac{1}{2}}(\partial B)$ to $\dot{H}^{\frac{1}{2}}(\partial B)$. Its restriction $\Lambda : \dot{L}^2(\partial B) \rightarrow \dot{L}^2(\partial B)$ is compact also.

Denote also by Λ_0 the *NtDm* for the problem (1.2) with the coefficient

$$\sigma(\mathbf{x}) = \sigma_B(\mathbf{x}), \text{ in } B, \quad (1.3)$$

and by u_0 the solution of the same problem. In this way u_0 represent the potential generated by the incoming current g in the domain B , when the inclusion D is not present. Let f_0 be the corresponding measured potential $f_0 = u_0|_{\partial B} = \Lambda_0 g$.

Moreover, we define the operator $\tilde{\Lambda}$ that will play a central role in the sequel:

$$\tilde{\Lambda} := \Lambda - \Lambda_0 : \dot{L}^2(\partial B) \rightarrow \dot{L}^2(\partial B). \quad (1.4)$$

Remark 2. The case $\sigma_D = 0$ and $\sigma_D = +\infty$ are allowed as well, and are known as perfectly insulating and perfectly conducting obstacles, but they require a slightly different treatment.

We will need also the Green function $N(\cdot, \boldsymbol{\xi}) \in \dot{L}^2(B)$, which is a solution of the following Neumann boundary-value problem with a singular source $\delta_{\boldsymbol{\xi}}$ centered in $\boldsymbol{\xi} \in B$:

$$\begin{cases} \nabla_1 \cdot (\sigma_B(\mathbf{x}) \nabla_1 N(\mathbf{x}, \boldsymbol{\xi})) = -\delta_{\boldsymbol{\xi}}(\mathbf{x}), & \mathbf{x} \in B, \\ \boldsymbol{\nu} \cdot \nabla_1 N(\mathbf{x}, \boldsymbol{\xi}) = -\frac{1}{|B|}, & \mathbf{x} \text{ on } \partial B. \end{cases} \quad (1.5)$$

Note that (1.5) does not embed any information about the inclusion D .

Denote by \mathbf{p} a two-dimensional vector (*i.e.* $|\mathbf{p}| = 1$). In the sequel we will often need the scalar product

$$\psi(\mathbf{x}, \boldsymbol{\xi}, \mathbf{p}) := \mathbf{p} \cdot \nabla_2 N(\mathbf{x}, \boldsymbol{\xi}), \quad \mathbf{x} \in B, \quad (1.6)$$

as well as its restriction on ∂B

$$l_{\boldsymbol{\xi}}^{\mathbf{p}} = \psi(\mathbf{x}, \boldsymbol{\xi}, \mathbf{p}) \Big|_{\mathbf{x} \text{ on } \partial B}. \quad (1.7)$$

Moreover, denoting with $\{\mathbf{e}_1, \mathbf{e}_2\}$ an orthonormal basis of \mathbb{R}^2 , we denote

$$l_{\boldsymbol{\xi}}^k = l_{\boldsymbol{\xi}}^{\mathbf{e}_k}, \quad k = 1, 2.$$

When the domain B is a circle with radius R there is an explicit formula for the solution $N(\mathbf{x}, \boldsymbol{\xi})$ of the Neumann problem (1.5) with $\sigma_B \equiv 1$ (see *e.g.* [2]):

$$N(\mathbf{x}, \boldsymbol{\xi}) = -\frac{1}{2\pi} \left(\log |\mathbf{x} - \boldsymbol{\xi}| + \log \left| \frac{R}{|\mathbf{x}|} \mathbf{x} - \frac{|\mathbf{x}|}{R} \boldsymbol{\xi} \right| \right) + \frac{\log R}{\pi}. \quad (1.8)$$

One can check that $N(\mathbf{x}, \boldsymbol{\xi}) \in \dot{H}^1(B \setminus \mathcal{O}_{\boldsymbol{\xi}})$, being $\mathcal{O}_{\boldsymbol{\xi}}$ an arbitrarily small neighbourhood of $\boldsymbol{\xi}$. See *e.g.* Theorem 2.

Notice that only the first logarithm can yield a singularity, since the second one is singular only when $\boldsymbol{\xi}$ falls on the boundary, *i.e.* if $|\mathbf{x}| \leq R$ and $|\boldsymbol{\xi}| < R$ then

$$\left| \frac{R}{|\mathbf{x}|} \mathbf{x} - \frac{|\mathbf{x}|}{R} \boldsymbol{\xi} \right| \geq \left| \frac{R}{|\mathbf{x}|} \mathbf{x} \right| - \left| \frac{|\mathbf{x}|}{R} \boldsymbol{\xi} \right| = \left| R - \frac{|\mathbf{x}| |\boldsymbol{\xi}|}{R} \right| > 0.$$

Moreover, one can check that $N(\cdot, \cdot)$ is a symmetric function.

In the case of (1.8) we have an explicit formula for the evaluation of ψ defined in (1.6) on the boundary of the unitary circle [6]:

$$\psi(\mathbf{x}, \boldsymbol{\xi}, \mathbf{p}) \Big|_{\partial B} = \frac{1}{\pi} \frac{\mathbf{p} \cdot (\boldsymbol{\xi} - \mathbf{x})}{|\boldsymbol{\xi} - \mathbf{x}|^2}, \quad \text{for } |\mathbf{x}| = 1. \quad (1.9)$$

2 Sampling Methods for EIT

The most famous sampling methods are the *Linear Sampling* (LS) and the *Factorization Method* (FM). The former was introduced in its modern form for scattering problems by *D.Colton et. al* in the middle '90, while the latter was introduced some years later by *A.Kirsch*. These methods can be classified as Shape Identification methods, since they allow to recover the shape of unknown contrast objects from indirect measurements.

Both LS and FM have been extended also to the EIT framework, and are widely studied in the literature nowadays. We will focus on the FM. The application of the FM applied to the Complete Electrode Model has been investigated in [15].

2.1 The case of small inclusions

Denote by $C_\delta(\boldsymbol{\xi}) \subset \mathbb{R}^2$ a circle centered in $\boldsymbol{\xi} \in \mathbb{R}^2$ with radius equal to δ .

Definition 1. Let $d_0 > 0$ be constant. Given M points $\boldsymbol{\xi}_1, \dots, \boldsymbol{\xi}_M$ in B such that $\text{dist}(\boldsymbol{\xi}_i, \boldsymbol{\xi}_j) \geq d_0, \forall i \neq j$, and $\text{dist}(\boldsymbol{\xi}_i, \partial B) \geq d_0, \forall j$, define for each j the inclusion $C_\delta(\boldsymbol{\xi}_j)$ with its coefficient σ_{D_j} . Define D as $D = \cup_{j=1}^M C_\delta(\boldsymbol{\xi}_j)$. The background coefficient σ_B can be inhomogeneous. If the parameter δ is small then we refer to this situation as small obstacle case. Under this assumption it is reasonable to assume the coefficient σ_{D_j} inside each inclusion to be homogeneous, but always satisfying Assumption 1.

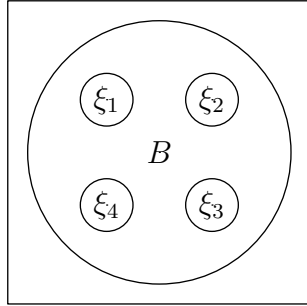


Fig. 2: Several obstacles which lie in a medium B . This figure displays $M = 4$ circle obstacles which are centered in $\boldsymbol{\xi}_1, \boldsymbol{\xi}_2, \boldsymbol{\xi}_3, \boldsymbol{\xi}_4$ and have a radius equal to δ .

The next result was first given in [9] under the strong assumption $\sigma(\mathbf{x}) \in C^\infty(B)$, and then extended in [7]. It relates the solutions $N(\mathbf{x}, \cdot)$ of problem (1.5) with the difference between the solution u of problem (1.2) with the coefficient (1.1) and the solution u_0 of the same problem (1.2) but with the coefficient (1.3).

Theorem 1. In the small obstacles case, when $\delta \downarrow 0$ the solution of problem (1.1) can be expanded as

$$u(\mathbf{x}) = u_0(\mathbf{x}) + \delta^2 \sum_{j=1}^M \lambda_j \nabla_1 N(\boldsymbol{\xi}_j, \mathbf{x}) \cdot M_j \nabla u_0(\boldsymbol{\xi}_j) + \mathcal{O}(\delta^{5/2}), \quad \forall \mathbf{x} \in \partial B, \quad (2.1)$$

with

$$\lambda_j = \sigma_B(\boldsymbol{\xi}_j) \frac{\sigma_B(\boldsymbol{\xi}_j) - \sigma_{D_j}}{\sigma_{D_j}}.$$

Here M_j is the polarization tensor corresponding to the j th inhomogeneity. It is a symmetric positive definite 2×2 matrix.

Corollary 1 (Corollary of Theorem 1). Under the Assumptions of Theorem 1, when $\sigma_B \equiv 1$ the expansion (2.1) for $\delta \downarrow 0$ holds with

$$\lambda_j = \frac{(1 - \sigma_{D_j})}{\sigma_{D_j}}.$$

Moreover, if the inclusion D_j has a circular shape then

$$M_j = |D_j| \begin{pmatrix} \frac{2\sigma_{D_j}}{1 + \sigma_{D_j}} & 0 \\ 0 & \frac{2\sigma_{D_j}}{1 + \sigma_{D_j}} \end{pmatrix}.$$

Remark 3. Denote by $E : \dot{L}^2(\partial B) \rightarrow \dot{L}^2(\partial B)$ the operator

$$Eg = \sum_{j=1}^M \lambda_j \nabla_1 N(\boldsymbol{\xi}_j, \cdot) \cdot M_j \nabla u_0(\boldsymbol{\xi}_j),$$

where $u_0 \in \dot{H}^1(B)$ is the solution of problem (1.2) with the coefficient (1.3). Then we can express $\tilde{\Lambda}$ introduced in (1.4) as

$$\tilde{\Lambda} = \delta^2 E + \mathcal{O}(\delta^{5/2}). \quad (2.2)$$

Theorem 2. The problem

$$\begin{cases} \Delta N(\mathbf{x}, \boldsymbol{\xi}) = -\delta_\xi(\mathbf{x}), & \mathbf{x} \in B, \\ \frac{\partial N(\mathbf{x}, \boldsymbol{\xi})}{\partial \boldsymbol{\nu}} = -\frac{1}{|B|}, & \mathbf{x} \text{ on } \partial B, \end{cases} \quad (2.3)$$

has a unique solution in $\dot{H}_{loc}^1(B \setminus \{\boldsymbol{\xi}\}) \cap L^2(B)$.

Proof of Theorem 2. Given $\boldsymbol{\xi} \in B$, the function

$$\phi(\cdot, \boldsymbol{\xi}) = -\frac{1}{2\pi} \log |\cdot - \boldsymbol{\xi}|$$

is a solution of the problem

$$\Delta \phi(\cdot, \boldsymbol{\xi}) = -\delta_\xi(\cdot), \text{ in } \mathbb{R}^2. \quad (2.4)$$

We observe that $\forall \varepsilon > 0$

$$\int_{\partial B} \frac{\partial \phi(\cdot, \boldsymbol{\xi})}{\partial \boldsymbol{\nu}} ds = \int_{|\mathbf{x}-\boldsymbol{\xi}|=\varepsilon} \frac{\partial \phi(\varepsilon e^\theta, \boldsymbol{\xi})}{\partial \boldsymbol{\nu}} \varepsilon d\theta = -\frac{\varepsilon}{2\pi} \int_0^{2\pi} \frac{1}{\varepsilon} = -1. \quad (2.5)$$

Now define the function $\varphi_N(\cdot, \boldsymbol{\xi}) = N(\cdot, \boldsymbol{\xi}) - \phi(\cdot, \boldsymbol{\xi})$, and consider the problem

$$\begin{cases} \Delta \varphi_N(\cdot, \boldsymbol{\xi}) = 0, & \text{in } B, \\ \frac{\partial \varphi_N(\cdot, \boldsymbol{\xi})}{\partial \boldsymbol{\nu}} = -\frac{\partial \phi(\cdot, \boldsymbol{\xi})}{\partial \boldsymbol{\nu}} - \frac{1}{|\partial B|}, & \text{on } \partial B, \end{cases} \quad (2.6)$$

which has a unique solution $\varphi_N \in \dot{H}^1(B)$ since, due to (2.5), $\frac{\partial \phi(\cdot, \boldsymbol{\xi})}{\partial \boldsymbol{\nu}} + \frac{1}{|\partial B|} \in \dot{H}^{-\frac{1}{2}}(\partial B)$. In addition $\varphi_N \in H^2(\partial B)$ because of the regularity on the boundary and $\frac{\partial \phi(\cdot, \boldsymbol{\xi})}{\partial \boldsymbol{\nu}} + \frac{1}{|\partial B|} \in \dot{H}^{\frac{1}{2}}(\partial B)$.

So we built a function

$$N(\cdot, \boldsymbol{\xi}) = \phi(\cdot, \boldsymbol{\xi}) + \varphi_N(\cdot, \boldsymbol{\xi})$$

which is a solution of problem (2.3). Moreover, we note that $N(\cdot, \boldsymbol{\xi}) \notin \dot{H}^1(B)$ due to the singularity in $\boldsymbol{\xi}$ of $\phi(\cdot, \boldsymbol{\xi})$. \square

2.1.1 Characterization of the support of the inclusions

In the case of small obstacles it is possible to characterize directly the support of the inclusions D through the range of the operator E . See [7] for the proof of the following theorem.

Theorem 3. $\text{Range}(E) = \text{span}\{l_{\boldsymbol{\xi}_j}^k, \quad j = 1, \dots, M, \quad k = 1, 2\}$.

Note that $\text{Range}(E)$ has finite dimension, since it is the span of $2M$ functions.

Theorem 4 (Unique continuation). *Let $O \subset \mathbb{R}^2$ be an open connected set. If the following conditions hold*

- $u \in C^2(O)$,
- $|\Delta u(\mathbf{x})| \leq C(|\nabla u(\mathbf{x})| + u(\mathbf{x})), \quad \forall \mathbf{x} \in O$,
- $u = 0$ in a neighbourhood of some $\mathbf{x}_0 \in O$,

then $u \equiv 0$ in O .

Theorem 5. Let $\mathbf{p} \in \mathbb{R}^2$, $|\mathbf{p}| = 1$. Then $l_\xi^p \in \text{Range}(E) \iff \xi \in \{\xi_j, j = 1, \dots, M\}$.

Proof of Theorem 5. Suppose that $\xi \notin \{\xi_j, j = 1, \dots, M\}$. If $l_\xi^p \in \text{Range}(E)$, then there exist a suitable g and a suitable \tilde{u} such that

$$l_\xi^p = Eg = \tilde{u}|_{\partial B}.$$

On the other side, the values \mathbf{p} and ξ in l_ξ^p uniquely determine the solution of problem (2.3), and thus the function ψ through (1.7). So $\psi|_{\partial B} = \tilde{u}|_{\partial B}$. From (2.1) we see that \tilde{u} is a linear combination with coefficients $\alpha_1, \dots, \alpha_M$ of the functions $\nabla_1 N(\xi_j, \mathbf{x})$,

$$\tilde{u}(\mathbf{x}) = \sum_{j=0}^M \alpha_j \nabla_1 N(\xi_j, \mathbf{x}), \quad (2.7)$$

and then we have also

$$\frac{\partial \psi}{\partial \nu} \Big|_{\partial B} = \frac{\partial \tilde{u}}{\partial \nu} \Big|_{\partial B}.$$

Therefore the function $w = \tilde{u} - \psi$ satisfies

$$\begin{cases} w = 0, & \text{on } \partial B, \\ \frac{\partial w}{\partial \nu} = 0, & \text{on } \partial B, \\ \Delta w = 0, & \text{in } B \setminus \{\xi, \xi_1, \dots, \xi_M\}, \end{cases} \quad (2.8)$$

and $w \in H_{loc}^2(B \setminus \{\xi, \xi_1, \dots, \xi_M\})$. Now take \tilde{w} such that

$$\begin{cases} \tilde{w} = 0, & \text{in } \mathbb{R}^2 \setminus B, \\ \tilde{w} = w, & \text{in } B \setminus \{\xi, \xi_1, \dots, \xi_M\}. \end{cases} \quad (2.9)$$

Then, denoting with $[\cdot]$ the jump, \tilde{w} also satisfies

$$\begin{aligned} [\tilde{w}] &= 0, \text{ on } \partial B, & \left[\frac{\partial \tilde{w}}{\partial \nu} \right] &= 0, \text{ on } \partial B, \\ \Delta \tilde{w} &= \begin{cases} 0, & \text{in } B \setminus \{\xi, \xi_1, \dots, \xi_M\}, \\ 0, & \text{in } \mathbb{R}^2 \setminus B. \end{cases} \end{aligned} \quad (2.10)$$

So in the end,

$$\begin{aligned} \Delta \tilde{w} &= 0, \text{ in } \mathbb{R}^2 \setminus \{\xi, \xi_1, \dots, \xi_M\}, \\ \tilde{w} &= 0, \text{ in } \mathbb{R}^2 \setminus B. \end{aligned}$$

Thanks to Theorem 4, $\psi = \tilde{u}$ in $B \setminus \{\xi, \xi_1, \dots, \xi_M\}$. Being O_ξ a neighbourhood of ξ that does not intersect $\{\xi_1, \dots, \xi_M\}$, we have a contradiction since $\tilde{u} \in H^1(O_\xi)$ (from (2.7)), but $\psi \notin H^1(O_\xi)$. The opposite implication is straightforward, from the characterization in Theorem 3. \square

See [7] for a detailed description of how to relate the range of the operators E and $\tilde{\Lambda}$, which are related each other by (2.2). In the next section we derive the characterization through the range of $\tilde{\Lambda}^{1/2}$ of the support of inclusions with arbitrary shape.

2.2 The Factorization Method for EIT

In this section we outline the basis of the FM applied to EIT. The main result is the factorization of the operator $\tilde{\Lambda}$ given in Theorem 6, (see [17, Chap.12,Thm.4] for a proof). In [14] a more general three-term factorization is derived for $\tilde{\Lambda} : \dot{H}^{-1/2}(\partial B) \rightarrow \dot{H}^{1/2}(\partial B)$. Also another simpler two-term factorization can be chosen, see *e.g.* [17]. Although many factorizations are possible, each of them provide a necessary and sufficient criterion to determine the inclusions. Lemma 1 and Theorem 9 show how this criterion becomes operative.

Let us introduce the operator $G : \dot{H}^{-1/2}(\partial D) \rightarrow \dot{L}^2(\partial B)$. It acts as a *Ntdm* of a suitable virtual problem,

$$\begin{cases} \nabla \cdot (\sigma_B(\mathbf{x})\nabla w) = 0, & \text{in } B \setminus \overline{D}, \\ \frac{\partial w}{\partial \nu} = 0, & \text{on } \partial B, \\ -\frac{\partial w}{\partial \nu} = \varphi, & \text{on } \partial D, \end{cases} \quad (2.11)$$

where $\varphi \in \dot{H}^{-1/2}(\partial D)$ is the input, and $w|_{\partial B} \in \dot{L}^2(\partial B)$ is the output. Moreover, define the space $W = \{w \in \dot{H}^1(B \setminus \overline{D}) : w \text{ solves (2.11)}\}$, and denote by $G^* : \dot{L}^2(\partial B) \rightarrow \dot{H}^{1/2}(\partial D)$ the adjoint of G . To define the operator T we introduce the problems

$$\begin{cases} \nabla \cdot (\sigma(\mathbf{x})\nabla \varpi) = 0, & \text{in } B \setminus \partial D, \\ \frac{\partial \varpi}{\partial \nu} = 0, & \text{on } \partial B, \\ [\varpi]_{\partial D} = \varphi, & \text{on } \partial D, \\ [\boldsymbol{\nu} \cdot \sigma(\mathbf{x})\nabla \varpi]_{\partial D} = 0, & \text{on } \partial D, \\ \int_{\partial B} \varpi \, ds = 0, \end{cases} \quad \begin{cases} \nabla \cdot (\sigma_B(\mathbf{x})\nabla \varpi_0) = 0, & \text{in } B \setminus \partial D, \\ \frac{\partial \varpi_0}{\partial \nu} = 0, & \text{on } \partial B, \\ [\varpi_0]_{\partial D} = \varphi, & \text{on } \partial D, \\ [\boldsymbol{\nu} \cdot \sigma_B(\mathbf{x})\nabla \varpi_0]_{\partial D} = 0, & \text{on } \partial D, \\ \int_{\partial B} \varpi_0 \, ds = 0. \end{cases} \quad (2.12)$$

The operator T is defined as

$$T : \dot{H}^{1/2}(\partial D) \rightarrow \dot{H}^{-1/2}(\partial D) : \varphi \mapsto \frac{\partial(\varpi^+ - \varpi_0^+)}{\partial \nu} \Big|_{\partial D},$$

where ϖ^+ and ϖ_0^+ are the restrictions of ϖ and ϖ_0 on $B \setminus \overline{D}$.

Theorem 6. *The operator $\tilde{\Lambda} : \dot{L}^2(\partial B) \rightarrow \dot{L}^2(\partial B)$ introduced in (1.4) can be factorized as*

$$\tilde{\Lambda} = GTG^*. \quad (2.13)$$

Theorem 7. *A point $\boldsymbol{\xi} \in B$ belongs to D if and only if $l_{\boldsymbol{\xi}}^p$ coincides with the trace of some potential $w \in W$.*

Proof. Let $\boldsymbol{\xi} \in D$. From the definition (1.7) we know that $l_{\boldsymbol{\xi}}^p$ is the trace of $\psi(\cdot, \boldsymbol{\xi}, \mathbf{p}) \in \dot{H}^1(B \setminus \overline{D})$. For every $\boldsymbol{\xi}$ the function $N(\cdot, \boldsymbol{\xi})$ has the same Neumann data on the boundary. Thus its normal derivative w.r.t. $\boldsymbol{\xi}$ is null on ∂B . Moreover, on each connected component of D , the *Green's formula* gives

$$\int_{\partial D_j} \nabla_2 \psi(\mathbf{x}, \boldsymbol{\xi}, \mathbf{p}) \cdot \boldsymbol{\nu} \, ds = 0, \quad (2.14)$$

for every component $D_j \subset D$ such that $\boldsymbol{\xi} \notin D_j$. But also the flux of $\psi(\cdot, \boldsymbol{\xi}, \mathbf{p})$ across $\partial(B \setminus \overline{D})$ vanishes, so (2.14) holds also for the component D_j of D such that $\boldsymbol{\xi} \in D_j$. Therefore $\psi(\cdot, \boldsymbol{\xi}, \mathbf{p}) \in W$.

In the case $\boldsymbol{\xi} \notin \overline{D}$, if $\exists w \in W$ such that $l_{\boldsymbol{\xi}}^p$ is the trace of w then we obtain a contradiction. In fact, w and $\psi(\cdot, \boldsymbol{\xi}, \mathbf{p})$ (related to $l_{\boldsymbol{\xi}}^p$ by (1.7)) satisfy the same Neumann problem in $B \setminus (\overline{D} \cup \{\boldsymbol{\xi}\})$

with the same boundary conditions. The uniqueness of the solution implies that w and $\psi(\cdot, \boldsymbol{\xi}, \mathbf{p})$ coincide in $B \setminus (\overline{D} \cup \{\boldsymbol{\xi}\})$. But now w extends harmonically into a neighbourhood $\mathcal{O}(\boldsymbol{\xi})$ of $\boldsymbol{\xi}$, so that w is bounded in $\mathcal{O}(\boldsymbol{\xi})$ while $\psi(\cdot, \boldsymbol{\xi}, \mathbf{p})$ is not.

If $\boldsymbol{\xi} \in \partial D$ with the same argument w and $\psi(\cdot, \boldsymbol{\xi}, \mathbf{p})$ coincide in $B \setminus (\overline{D})$. But this is a contradiction because $w \in \dot{H}^1(\mathcal{O}(\boldsymbol{\xi}) \cap (B \setminus (\overline{D})))$, but $\psi(\cdot, \boldsymbol{\xi}, \mathbf{p})$ has the singularity in $\boldsymbol{\xi}$. \square

Lemma 1. *A point $\boldsymbol{\xi} \in B$ belongs to D if and only if $l_{\boldsymbol{\xi}}^p \in \text{Range}(G)$.*

Proof. For any $\varphi \in \dot{H}^{-1/2}(\partial D)$ the problem (2.11) has a unique solution $w \in W$. Vice-versa, every function $w \in W$ is a solution of problem (2.11), with a well-defined normal derivative $\varphi \in \dot{H}^{-1/2}(\partial D)$. The thesis follows as a consequence of Theorem 7. \square

Remark 4. *The space $\dot{H}^{1/2}(\partial D)$ is a Banach reflexive space, with dual containing $\dot{H}^{-1/2}(\partial D)$.*

Theorem 8. *The operator $T : \dot{H}^{1/2}(\partial D) \rightarrow \dot{H}^{-1/2}(\partial D)$ is self adjoint and coercive over $\dot{H}^{1/2}(\partial D)$.*

Theorem 9. *Let $\tilde{\Lambda} : \dot{L}^2(\partial B) \rightarrow \dot{L}^2(\partial B)$ and $G : \dot{H}^{-1/2}(\partial D) \rightarrow \dot{L}^2(\partial B)$ and $T : \dot{H}^{1/2}(\partial D) \rightarrow \dot{H}^{-1/2}(\partial D)$. In addition, let G be injective with dense range and let T be self adjoint and coercive on $\text{Range}(G^*)$. Then $\text{Range}(G) = \text{Range}(\tilde{\Lambda}^{1/2})$ and*

$$y \in \text{Range}(G) \iff \sum_{j=1}^{\infty} \frac{|(y, y_j)_Y|^2}{\lambda_j} < \infty, \quad (2.15)$$

where $\{\lambda_j, y_j : j \in J\}$ denotes a spectral system of the self adjoint and compact operator $\tilde{\Lambda} = GTG^*$.

See [17, Chap.12] for the proof of Theorems 6, 8, 9.

2.3 Inhomogeneous background

Here we show our approach to numerically solve the singular problem (1.5) when the coefficient σ_B is inhomogeneous. To overcome the singularity in the forcing term, we resort to the fundamental solution

$$\phi(\cdot, \boldsymbol{\xi}) = -\frac{1}{2\pi\sigma_B(\boldsymbol{\xi})} \log \left| \cdot - \boldsymbol{\xi} \right|, \quad \mathbf{x} \in \mathbb{R}^2, \quad (2.16)$$

of the problem

$$-\nabla \cdot \left(\sigma_B(\boldsymbol{\xi}) \nabla \phi(\cdot, \boldsymbol{\xi}) \right) = \delta_{\boldsymbol{\xi}}, \quad \text{in } \mathbb{R}^2. \quad (2.17)$$

Since the singularity at $\boldsymbol{\xi}$ in problem (1.5) is of the same kind as in problem (2.17), we can restrict problem (1.5) in a small neighbourhood $\mathcal{O}(\boldsymbol{\xi}) \subset \mathbb{R}^2$ of $\boldsymbol{\xi}$ where

$$\sigma_B(\mathbf{x}) \approx \sigma_B(\boldsymbol{\xi}), \quad \forall \mathbf{x} \in \mathcal{O}(\boldsymbol{\xi}),$$

and approximate the solution $N(\mathbf{x}, \boldsymbol{\xi})$ of problem (1.5) near the singularity in $\boldsymbol{\xi}$ as

$$N(\mathbf{x}, \boldsymbol{\xi}) \approx \phi(\mathbf{x}, \boldsymbol{\xi}), \quad \forall \mathbf{x} \in \mathcal{O}(\boldsymbol{\xi}).$$

Then we can write a nonsingular problem for the difference

$$\varphi_N(\cdot, \boldsymbol{\xi}) = N(\cdot, \boldsymbol{\xi}) - \phi(\cdot, \boldsymbol{\xi}), \quad (2.18)$$

plugging (2.18) in (1.5):

$$\begin{cases} -\nabla_x \cdot \left(\sigma_B(\mathbf{x}) \nabla_1 \varphi_N(\mathbf{x}, \boldsymbol{\xi}) \right) = -\nabla_x \cdot \left(\left(\sigma_B(\boldsymbol{\xi}) - \sigma_B(\mathbf{x}) \right) \nabla_1 \phi(\mathbf{x}, \boldsymbol{\xi}) \right), & \mathbf{x} \text{ in } B, \\ \sigma_B(\mathbf{x}) \nabla_1 \varphi_N(\mathbf{x}, \boldsymbol{\xi}) \cdot \boldsymbol{\nu} = -\sigma_B(\mathbf{x}) \nabla_1 \phi(\mathbf{x}, \boldsymbol{\xi}) \cdot \boldsymbol{\nu} - \frac{1}{|\partial B|}, & \mathbf{x} \text{ on } \partial B. \end{cases} \quad (2.19)$$

The forcing term in this problem still contains the term $\nabla_1\phi(\cdot, \boldsymbol{\xi})$ which blows up approaching $\boldsymbol{\xi}$, but now it is multiplied by a vanishing coefficient. Moreover, the weak formulation of (2.23) reads

$$\begin{aligned} \text{find } \varphi_N \in \dot{H}^1(B) \text{ such that } \int_B \sigma_B(\mathbf{x}) \nabla_1 \varphi_N(\mathbf{x}, \boldsymbol{\xi}) \cdot \nabla v \, d\mathbf{x} &= \int_B \left(\sigma_B(\boldsymbol{\xi}) - \sigma_B(\mathbf{x}) \right) \nabla_1 \phi(\mathbf{x}, \boldsymbol{\xi}) \cdot \nabla v \, d\mathbf{x} + \\ &+ \int_{\partial B} \left(-\sigma_B(\boldsymbol{\xi}) \nabla_1 \phi(\mathbf{x}, \boldsymbol{\xi}) \cdot \boldsymbol{\nu} - \frac{1}{|\partial B|} \right) v \, ds, \quad \forall v \in H^1(B). \end{aligned} \quad (2.20)$$

Lemma 2. *If $\sigma_B(\cdot)$ is α -Holderian in B with $\alpha > 0$, i.e. $\exists 0 < K < \infty$ such that*

$$|\sigma_B(\mathbf{x}_1) - \sigma_B(\mathbf{x}_2)| \leq K |\mathbf{x}_1 - \mathbf{x}_2|^\alpha, \quad \forall \mathbf{x}_1, \mathbf{x}_2 \in B, \quad (2.21)$$

then the linear functional

$$F(w) = \int_B \left(\sigma_B(\boldsymbol{\xi}) - \sigma_B(\mathbf{x}) \right) \nabla_1 \phi(\mathbf{x}, \boldsymbol{\xi}) \cdot \nabla w \, d\mathbf{x},$$

is bounded on $H^1(B)$.

Proof of Lemma 2. The function $\zeta(\mathbf{x}) = \left(\sigma_B(\boldsymbol{\xi}) - \sigma_B(\mathbf{x}) \right) \nabla_1 \phi(\mathbf{x}, \boldsymbol{\xi})$ belongs to $L^2(B)$ if $\alpha > 0$, thus

$$|F(w)| = \left| \int_B \zeta(\mathbf{x}) \cdot \nabla w \, d\mathbf{x} \right| \leq \|\zeta\|_{L^2(B, \mathbb{R}^2)} \|\nabla w\|_{L^2(B, \mathbb{R}^2)}, \quad \forall w \in H^1(B).$$

□

In the quantity ψ defined in (1.6), the dependence of $N(\cdot, \cdot)$ on the second argument is smooth. So we can exploit this regularity to derive a numerical scheme that given $\boldsymbol{\xi} \in B$ directly computes $\nabla_2 N(\cdot, \boldsymbol{\xi})$. To this aim we differentiate (2.18) with respect to the second argument, and obtain

$$\nabla_2 \varphi_N(\cdot, \boldsymbol{\xi}) = \nabla_2 N(\cdot, \boldsymbol{\xi}) - \nabla_2 \phi(\cdot, \boldsymbol{\xi}). \quad (2.22)$$

Since $\psi(\cdot, \boldsymbol{\xi}, \mathbf{p})$ is a solution of problem (1.5) for any \mathbf{p} , then we can derive a numerical scheme to compute $\nabla_2 N(\cdot, \boldsymbol{\xi})$. The derivatives of ϕ w.r.t. $\boldsymbol{\xi}$ are

$$\frac{\partial \phi(\cdot, \boldsymbol{\xi})}{\partial \xi_k} = \frac{1}{2\pi\sigma_B(\boldsymbol{\xi})^2} \frac{\partial \sigma_B(\boldsymbol{\xi})}{\partial \xi_k} \log(|\mathbf{x} - \boldsymbol{\xi}|) + \frac{x_k - \xi_k}{2\pi\sigma_B(\boldsymbol{\xi})|\mathbf{x} - \boldsymbol{\xi}|^2}, \quad k = 1, 2,$$

and since ϕ is analytical when $\mathbf{x} \neq \boldsymbol{\xi}$ then the mixed derivatives coincide:

$$\begin{aligned} \frac{\partial^2 \phi(\mathbf{x}, \boldsymbol{\xi})}{\partial x_1 \partial \xi_1} &= \frac{1}{2\pi\sigma_B(\boldsymbol{\xi})^2} \frac{\partial \sigma_B(\boldsymbol{\xi})}{\partial \xi_1} \frac{x_1 - \xi_1}{|\mathbf{x} - \boldsymbol{\xi}|^2} + \frac{(x_2 - \xi_2)^2 - (x_1 - \xi_1)^2}{2\pi\sigma_B(\boldsymbol{\xi})|\mathbf{x} - \boldsymbol{\xi}|^4}, \\ \frac{\partial^2 \phi(\mathbf{x}, \boldsymbol{\xi})}{\partial x_2 \partial \xi_1} &= \frac{1}{2\pi\sigma_B(\boldsymbol{\xi})^2} \frac{\partial \sigma_B(\boldsymbol{\xi})}{\partial \xi_1} \frac{x_2 - \xi_2}{|\mathbf{x} - \boldsymbol{\xi}|^2} - \frac{(x_1 - \xi_1)(x_2 - \xi_2)}{\pi\sigma_B(\boldsymbol{\xi})|\mathbf{x} - \boldsymbol{\xi}|^4}, \\ \frac{\partial^2 \phi(\mathbf{x}, \boldsymbol{\xi})}{\partial x_1 \partial \xi_2} &= \frac{1}{2\pi\sigma_B(\boldsymbol{\xi})^2} \frac{\partial \sigma_B(\boldsymbol{\xi})}{\partial \xi_2} \frac{x_1 - \xi_1}{|\mathbf{x} - \boldsymbol{\xi}|^2} - \frac{(x_2 - \xi_2)(x_1 - \xi_1)}{\pi\sigma_B(\boldsymbol{\xi})|\mathbf{x} - \boldsymbol{\xi}|^4}, \\ \frac{\partial^2 \phi(\mathbf{x}, \boldsymbol{\xi})}{\partial x_2 \partial \xi_2} &= \frac{1}{2\pi\sigma_B(\boldsymbol{\xi})^2} \frac{\partial \sigma_B(\boldsymbol{\xi})}{\partial \xi_2} \frac{x_2 - \xi_2}{|\mathbf{x} - \boldsymbol{\xi}|^2} + \frac{(x_1 - \xi_1)^2 - (x_2 - \xi_2)^2}{2\pi\sigma_B(\boldsymbol{\xi})|\mathbf{x} - \boldsymbol{\xi}|^4}. \end{aligned}$$

Denoting by superscript the partial derivative, we have two problems for the unknowns $\varphi_N^k = \partial \varphi_N / \partial \xi_k$, $k = 1, 2$:

$$\begin{cases} -\nabla_x \cdot \left(\sigma_B(\mathbf{x}) \nabla_1 \varphi_N^k(\mathbf{x}, \boldsymbol{\xi}) \right) = -\nabla_x \cdot \left(\left(\sigma_B(\boldsymbol{\xi}) - \sigma_B(\mathbf{x}) \right) \boldsymbol{\Phi}^k(\mathbf{x}, \boldsymbol{\xi}) \right), & \mathbf{x} \text{ in } B, \\ \sigma_B(\mathbf{x}) \nabla_1 \varphi_N^k(\mathbf{x}, \boldsymbol{\xi}) \cdot \boldsymbol{\nu} = -\sigma_B(\mathbf{x}) \boldsymbol{\Phi}^k(\mathbf{x}, \boldsymbol{\xi}) \cdot \boldsymbol{\nu} - \frac{1}{|\partial B|}, & \mathbf{x} \text{ on } \partial B, \end{cases} \quad (2.23)$$

with

$$\Phi^k(\mathbf{x}, \boldsymbol{\xi}) = \left(\frac{\partial^2 \phi(\mathbf{x}, \boldsymbol{\xi})}{\partial x_1 \partial \xi_k}, \frac{\partial^2 \phi(\mathbf{x}, \boldsymbol{\xi})}{\partial x_2 \partial \xi_k} \right), \quad \forall (\mathbf{x}, \boldsymbol{\xi}) \in B \times B : \mathbf{x} \neq \boldsymbol{\xi}.$$

Remark 5. All the second derivatives of ϕ are singular in $\mathbf{x} = \boldsymbol{\xi}$, and behave like $1/|\mathbf{x} - \boldsymbol{\xi}|^2$. Therefore, we can proceed as in Lemma 2 to show that the functional in (2.23) is bounded over $H^1(B)$, under the assumption $\alpha > 1$ in (2.21).

3 Regularization techniques

In section 2.2 we showed the basis of the FM. Now we present some operative criteria to implement the range test. They are all based on the SVD decomposition of the operator $\tilde{\Lambda}^{1/2}$. We focus mainly on *Tikhonov Regularization* (TR), although also a straightforward application of the *Picard Criterion* in (2.15) can give good results.

Algorithm 1 The Factorization Method for EIT

Sample the probed region B with a set of points $R = \{\mathbf{y}_j\}_{j=1}^P$

for \mathbf{y} in the set R **do**

solve problem (1.5) to find its solution $N(\cdot, \mathbf{y})$,

compute l_y^k from $N(\cdot, \mathbf{y})$ using (1.7),

exploiting the informations in l_y^k , decide if \mathbf{y} belongs or not to D .

end for

The SVD decomposition of a real matrix $A \in \mathbb{R}^{m \times n}$ is

$$A = U \Sigma V^*, \quad (3.1)$$

where $U \in \mathbb{R}^{m \times m}$ and $V \in \mathbb{R}^{n \times n}$ are unitary matrices and $\Sigma \in \mathbb{R}^{m \times n}$ is a diagonal matrix containing the singular values σ_i , with $1 \leq i \leq \min(m, n)$. The columns of $U = (u_1 | \dots | u_m)$ and $V = (v_1 | \dots | v_n)$ are the singular vectors u_i, v_i which solve

$$A v_i = \sigma_i u_i, \quad \text{and} \quad A^* u_i = \sigma_i v_i.$$

3.1 Tikhonov regularization

In this section we need the adjoint of the operator $\tilde{\Lambda}^{1/2}$, where $\tilde{\Lambda}$ is defined in (1.4). To simplify the notation we rename it as $M = \tilde{\Lambda}^{1/2}$.

To check whether a given l_ξ^k belongs to $\text{Range}(M)$ we have to solve the problem

$$M g_\xi^k = l_\xi^k, \quad (3.2)$$

which demands for regularization. The keypoint is

$$\boldsymbol{\xi} \in D \iff \left(\|g_\xi^k\|_{L^2(\partial B)} \right)^{-1} = 0.$$

The TR of (3.2) reads

$$\left(\alpha + M^* M \right) g_\xi^k = M^* l_\xi^k. \quad (3.3)$$

In our case we choose the *Fourier basis* to discretize the operator M . It corresponds to take input currents in $\dot{L}^2(\partial B)$ instead of $\dot{H}^{-\frac{1}{2}}(\partial B)$. Accordingly the voltage will belong to $H^{\frac{3}{2}}(B)$, and thus our measured voltage will be in $H^1(\partial B)$ at least.

Since we discretize l_ξ^k and g_ξ^k in (3.2) over the same orthogonal basis, then the discretization of M is a square matrix. This is a good choice in the case of the *Continuous Model*, but not for other models (e.g. the *Complete Electrode Model*).

In the sequel we denote by σ_i the singular values of M and by u_i and v_i the corresponding left and right singular vectors. Both the sets $\{u_i\}_{i=1}^\infty$ and $\{v_i\}_{i=1}^\infty$ are an orthonormal basis of $L^2(\partial B)$. Thus for any $\eta \in L^2(\partial B)$ we have:

$$M\eta = \sum_{i=1}^{\infty} \sigma_i(\eta, v_i)u_i, \quad M^*\eta = \sum_{i=1}^{\infty} \sigma_i(\eta, u_i)v_i, \quad (M^*M)\eta = \sum_{i=1}^{\infty} \sigma_i^2(\eta, v_i)v_i,$$

and applying this to problem (3.3) we get

$$M^*l_\xi^k = \sum_{i=1}^{\infty} \sigma_i(l_\xi^k, u_i)v_i, \quad (M^*M)g_\xi^k = \sum_{i=1}^{\infty} \sigma_i^2(g_\xi^k, v_i)v_i,$$

as well as the regularized solution

$$g_\xi^k = \sum_{i=1}^{\infty} \frac{\sigma_i}{\alpha + \sigma_i^2} (l_\xi^k, u_i)v_i.$$

We choose the regularization parameter α using *Morozov principle*, i.e. imposing

$$\|Mg_\xi^k - l_\xi^k\|_{L^2(\partial B)} \leq \delta, \quad (3.4)$$

with the parameter $\delta > 0$ to be somehow related to the accuracy of the measures. We pick

$$\delta = \gamma\sigma_1, \quad (3.5)$$

being σ_1 the largest singular value of M , and γ a given threshold. The terms l_ξ^k depends on ξ , so to guarantee that (3.4) is uniformly satisfied we normalize l_ξ^k as $\hat{l}_\xi^k = l_\xi^k / \|l_\xi^k\|_{L^2(\partial B)}$. Since

$$\|Mg_\xi^k - \hat{l}_\xi^k\|_{L^2(\partial B)}^2 = \sum_{i=1}^{\infty} \left(\frac{\sigma_i^2}{\alpha + \sigma_i^2} - 1 \right)^2 (\hat{l}_\xi^k, u_i)^2 = \sum_{i=1}^{\infty} \left(\frac{\alpha}{\alpha + \sigma_i^2} \right)^2 (\hat{l}_\xi^k, u_i)^2,$$

to impose (3.4) we solve the (truncated version of the) nonlinear equation

$$f(\alpha) := \sum_{i=1}^{\infty} \frac{\alpha^2}{(\alpha + \sigma_i^2)^2} (\hat{l}_\xi^k, u_i)^2 - \delta^2 = 0. \quad (3.6)$$

The function $\alpha \mapsto \|Mg_\xi^k - \hat{l}_\xi^k\|_{L^2(\partial B)}$ is monotonically increasing w.r.t. α . If δ is sufficiently small then the solutions of (3.6) lie in a non-empty closed interval, see [10] for the proof.

3.2 Picard criterion

Another criterion to test the range condition is analyzed in [12]. It employs the function:

$$I_k(\xi) = \frac{1}{\|l_\xi^k\|_{L^2(\partial B)}^2} \sum_{i=1}^{\infty} \frac{|(l_\xi^k, u_i)_{L^2(\partial B)}|^2}{|\sigma_i|}, \quad (3.7)$$

and it reads

$$\xi \in D \iff I_k(\xi) < \infty.$$

The function (3.7) can be approximated by $\tilde{I}_k(\xi) \approx I_k(\xi)$ with

$$\tilde{I}_k(\xi) = \sum_{i=1}^m \frac{|(l_\xi^k, u_i)_{L^2(\partial B)}|^2}{|\sigma_i|} \bigg/ \sum_{i=1}^m |(l_\xi^k, u_i)_{L^2(\partial B)}|^2, \quad (3.8)$$

retaining only the m greatest singular values above the expected measurement error. Note that the normalization of l_ξ^k is already embedded in (3.7). We refer to this criterion as *Picard Criterion* (PC). It does not require to solve problem (3.2) to find its regularized solution.

3.3 Algebraic formulation

Here we explain the steps to derive the algebraic formulation of problem (3.2) regularized with Tikhonov. Starting from (3.3) and using the SVD decomposition of $M = U\Sigma V^*$ we get $M^*\hat{\Lambda} = V\Sigma U^*U\Sigma V^* = V\Sigma^2 V^*$, and $M^*\hat{l}_y^k = V\Sigma U^*\hat{l}_y^k$, so that from (3.3) it follows

$$\left(\alpha I + V\Sigma^2 V^*\right)g_y^k = \left(\alpha VV^* + V\Sigma^2 V^*\right)g_y^k = V\left(\alpha I + \Sigma^2\right)V^*g_y^k = V\Sigma U^*\hat{l}_y^k.$$

Defining the diagonal matrix R_α as

$$[R_\alpha]_{i,i} = \frac{\Sigma_{i,i}}{(\alpha + \Sigma_{i,i}^2)} \quad (3.9)$$

we get $V^*g_y^k = R_\alpha U^*\hat{l}_y^k$, or equivalently $g_y^k = VR_\alpha U^*\hat{l}_y^k$.

4 Numerical results

To show the results, we display the isolines of the indicator function

$$C(\boldsymbol{\xi}) = \left(\log \left(v_1(\boldsymbol{\xi}) + v_2(\boldsymbol{\xi}) \right) \right)^{-1}, \quad (4.1)$$

where $v_k(\boldsymbol{\xi}) = \|g_\xi^k\|_{L^2(\partial B)}$ in the case of TR, or $v_k(\boldsymbol{\xi}) = \tilde{I}_k(\boldsymbol{\xi})$ in the case of PC. A crucial point is the tuning of the scale and the choice of the isovalue that represent the obstacle. In practice, this requires additional informations on the value of the coefficient in the inclusions. We plot the isolines of $C(\boldsymbol{\xi})$ in the range

$$\left[C_{\min}^f, C_{\max} \right] := \left[f \cdot \min\{C(\boldsymbol{\xi}) : \boldsymbol{\xi} \in D\}, \max\{C(\boldsymbol{\xi}) : \boldsymbol{\xi} \in D\} \right],$$

using the parameter $0 < f < 1$. The step between the isolines is kept fixed, and this provide informations also on the gradient of the indicator function. In all the numerical tests, the domain B is the unitary ball centered in $(0, 0)$. The sampling points consist in a 50×50 uniform grid over the square $[-1, 1] \times [-1, 1]$. In the FM we use only the points that fall 0.05 farther from ∂B . In the testcases with small obstacles the resolution is increased to 100×100 . The dashed purple line always marks the exact geometry of the obstacle(s).

As will be explained in the sequel, we need also to display the value of the indicator function (4.1). Thus we report also the plots with a color scale associated to the value of C .

4.1 The homogeneous case

The tests featuring an homogeneous background $\sigma_B = 1$ and $\sigma_D = 2$ are named with uppercase letters:

- *testcase A*: circular obstacle with radius 0.3 centered in $(0.3, 0.1)$;
- *testcase B*: ten small circular obstacles with radius 0.025;
- *testcase C*: two circular obstacles with radius 0.2 centered in $(-0.35, -0.35)$ and $(0.35, 0.35)$;
- *testcase D*: ellipsoidal obstacle centered in $(0.3, 0.1)$, with semiaxes 0.1 and 0.3.

Figure 3 displays the singular values of $\tilde{\Lambda}^{1/2}$ in the aforementioned testcases. Then, Figures 4, 5, 6, 7 show the isolines of the indicator function (4.1) employing TR or PC. The testcase A is classic and does not show any significative differences between TR and PC. If the parameter γ is too low then the isolines exhibits oscillations because the instability due to ill-posedness shows up.

In the testcase C the TR is less sensitive to the mutual disturbance between the two obstacles. Also in testcase D, the TR allows to recover the elongated shape, while PC tends to reconstruct a circle. In the testcase B both TR and PC can locate the outer inclusions, although TR is more accurate and provides some informations for the internal inclusions as well. See also a detailed zoom of the isolines near the obstacle in Figures 27, 28, 29, 30.

In the homogeneous case, it is possible to clearly detect the obstacle directly looking at the values of the optimal regularization parameter $\alpha = \alpha(\xi)$ which solves (3.6).

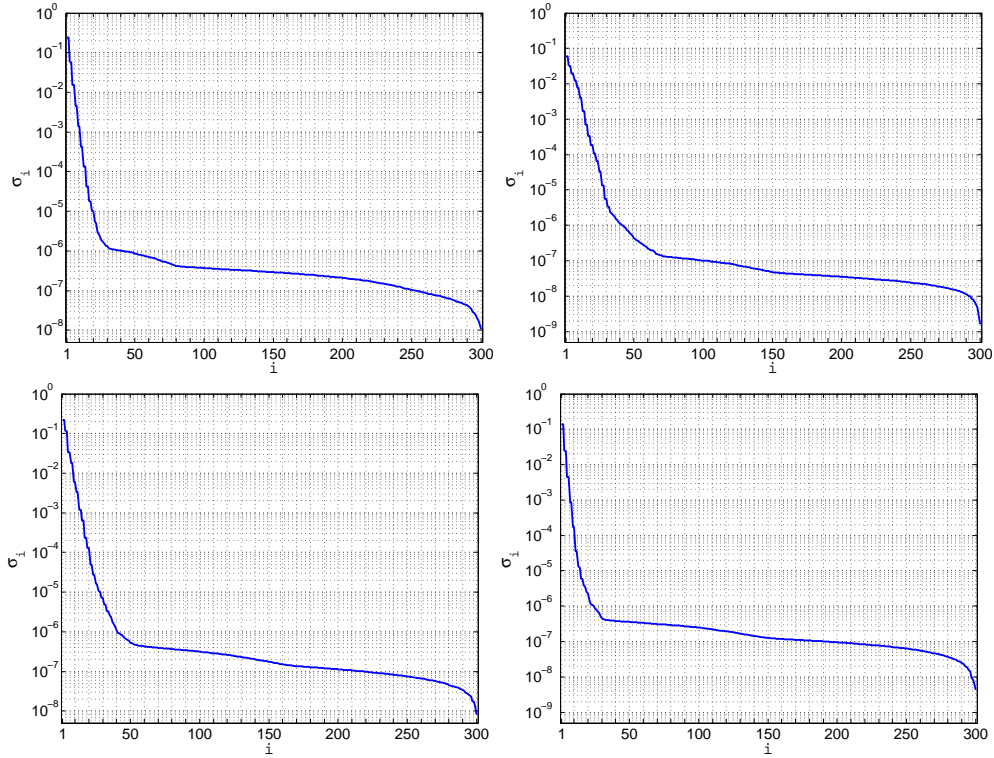


Fig. 3: Singular values σ_i of $\tilde{\Lambda}^{1/2}$. Testcase A (top-left). Testcase B (top-right). Testcase C (bottom-left). Testcase D (bottom-right).

4.2 The inhomogeneous case

We proceed to test our numerical scheme (2.23) in some cases featuring an inhomogeneous background. Let us name with roman numbers the following tests:

- *testcase I*: piece-wise constant conductivity defined as in Fig. 9-Left. The radius of the concentric circle is 0.7. The obstacle is a circle with radius 0.1 centered in $(0.35, 0.35)$ and $\sigma_D = 1e - 3$.
- *testcase II*: piece-wise constant conductivity defined as in Fig. 9-Right. The obstacle falls across the interface where the value of σ_B jumps by one order of magnitude. The radius of the concentric circles are 0.35 and 0.75. The obstacle is a circle with radius 0.1 centered in $(0, 0.33)$ and $\sigma_D = 1e - 3$.
- *testcase IIIa*: $\sigma_B = 1 + \beta(\sin(5x) + \cos(5y))$, $\beta = 0.15$. The obstacle is a circle with radius 0.15 centered in $(-0.3, 0.3)$ and $\sigma_D = 2$.
- *testcase IIIb*: same as Testcase IIIa but with $\beta = 0.25$.

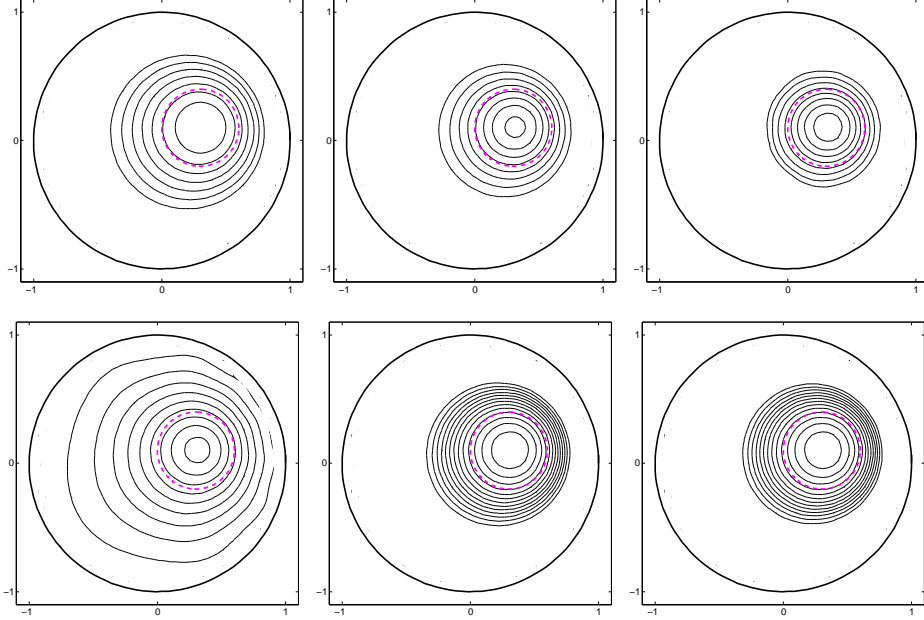


Fig. 4: Testcase A. Isolines of $C(\xi)$ in $[C_{\min}^{0.5}, C_{\max}]$. Top: Tikhonov regularization: $\gamma = 5e - 1$ (left), $\gamma = 5e - 2$ (center), $\gamma = 5e - 3$ (right). Bottom: Picard criterion, $m = 5$ (left), $m = 25$ (center), $m = 50$ (right).

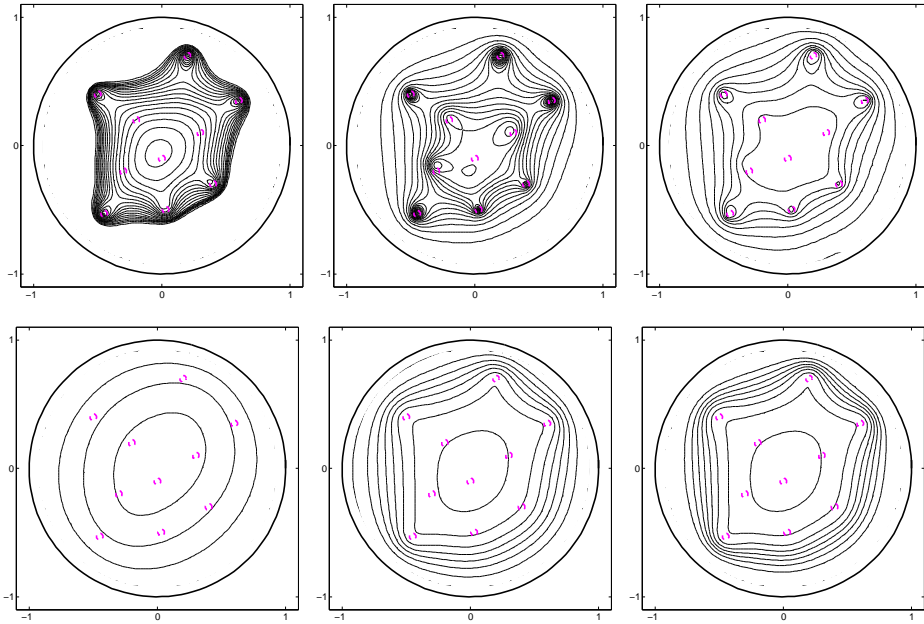


Fig. 5: Testcase B. Isolines of $C(\xi)$ in $[C_{\min}^{0.5}, C_{\max}]$. Top: Tikhonov regularization, $\gamma = 1e - 2$ (left), $\gamma = 1e - 3$ (center), $\gamma = 1e - 4$ (right). Bottom: Picard criterion, $m = 10$ (left), $m = 25$ (center), $m = 50$ (right).

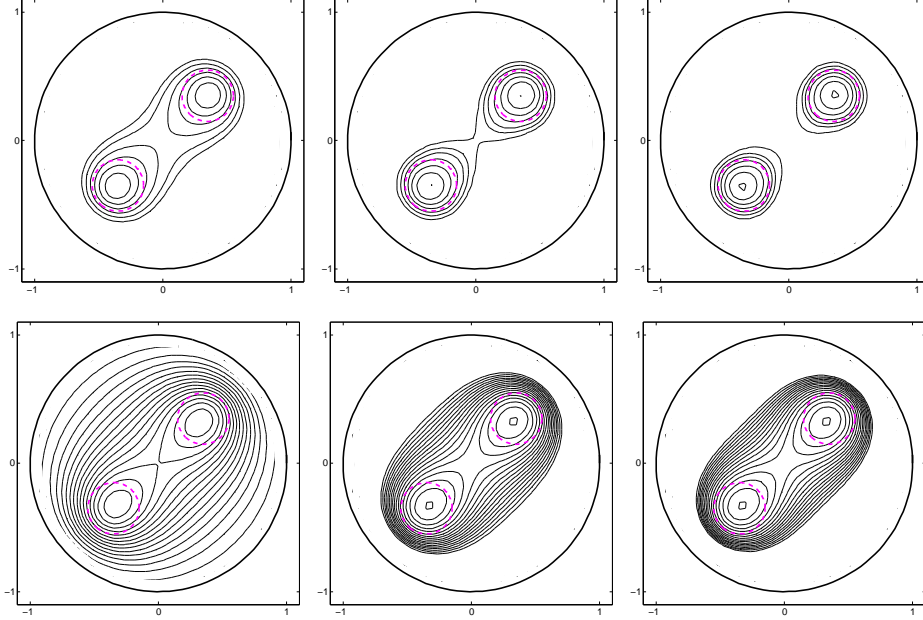


Fig. 6: Testcase C. Isolines of $C(\xi)$ in $[C_{\min}^{0.6}, C_{\max}]$. Top: Tikhonov regularization with $\gamma = 5e - 3$ (left), $\gamma = 1e - 3$ (center), $\gamma = 5e - 4$ (right). Bottom: Picard criterion. $m = 10$ (left), $m = 25$ (center), $m = 50$ (right).

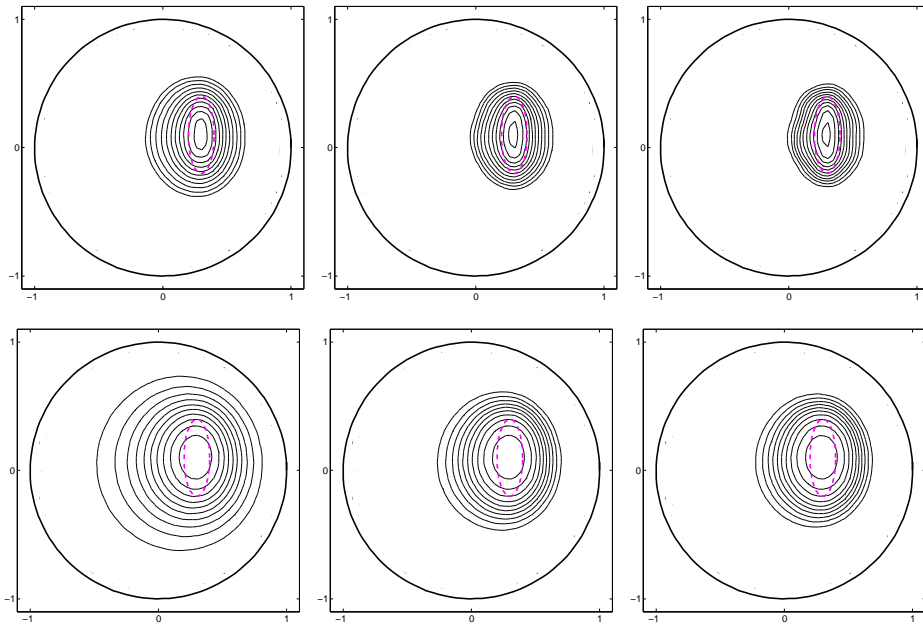


Fig. 7: Testcase D. Isolines of $C(\xi)$ in $[C_{\min}^{0.5}, C_{\max}]$. Top: Tikhonov regularization with $\gamma = 5e - 2$ (left), $\gamma = 1e - 2$ (center), $\gamma = 5e - 3$ (right). Bottom: Picard criterion. $m = 10$ (left), $m = 25$ (center), $m = 50$ (right).

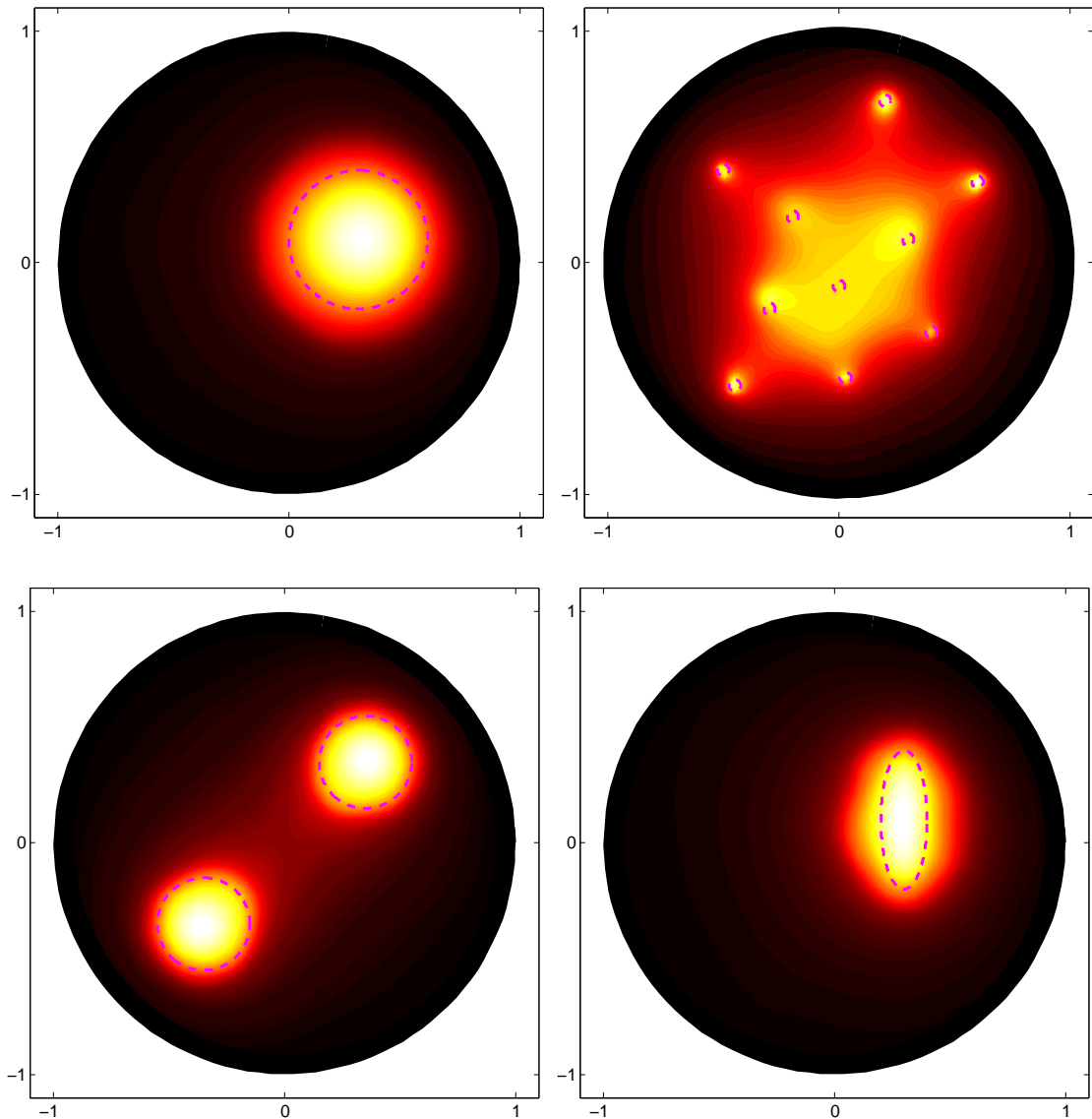


Fig. 8: Tikhonov regularization. Testcase A, $\gamma = 5e - 3$ (top-left). Testcase B, $\gamma = 1e - 3$ (top-right). Testcase C, $\gamma = 5e - 4$ (bottom-left). Testcase D, $\gamma = 5e - 3$ (bottom-right).

- *testcase IVa*: ten small circular obstacles with radius (0.025) , $\sigma_B = 1 + \beta(\sin(5x) + \cos(5y))$, $\beta = 0.25$ and $\sigma_D = 2$.
- *testcase IVb*: same as Testcase IVa but with $\beta = 0.3$.
- *testcase V*: one small circular obstacle with radius 0.025 centered in $(-0.3, 0.3)$, $\sigma_B = 5 \cdot (x + y) + 11$ and $\sigma_D = 1e - 3$.
- *testcase VI*: $\sigma_B = 1 + (x^2 + y^2)$, $\sigma_D = 1e - 3$. The obstacle is a circle with radius 0.15 centered in $(-0.3, 0.3)$.

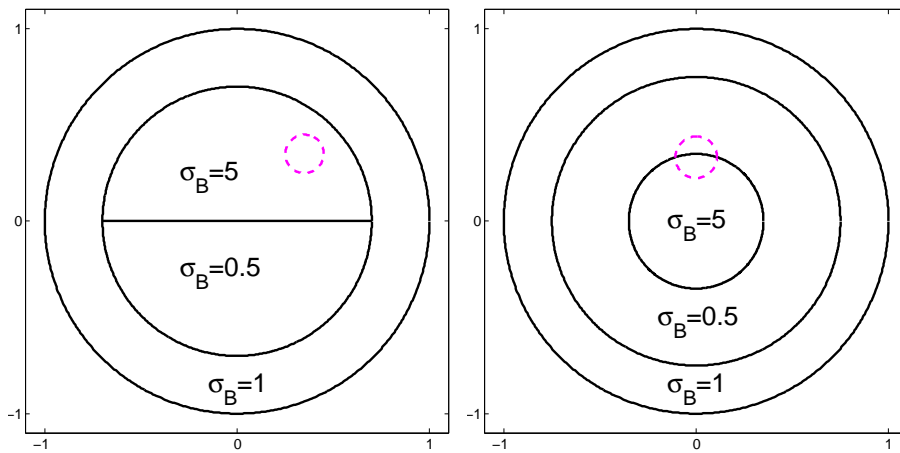


Fig. 9: Values of σ_B in the Testcase I (left) and in the Testcase II (right).

Again, we display the singular values of $\tilde{\Lambda}^{1/2}$ for all the testcases in Figures 10, 15. Despite the differences among the geometries and values of σ_B in the testcases, the singular values behave likewise. The most important difference is the order of magnitude of the greatest singular values, since this affects the choice of the regularization parameters.

The numerical scheme (2.23) performs very well in the testcases I,II with a piece-wise constant conductivity. In both cases σ_B has a jump by one order of magnitude. In the figures 11,12 we reconstruct the obstacle using Tychonov regularization and the Picard criterion. Figures 31,32,33-Left show a zoom of the isolines near the obstacle.

In the testcases IIIa the coefficient σ_B has a $\pm 30\%$ variation, and Figure 13 shows that both TR and PC are capable of accurately detecting shape and location of the obstacle. See also in Figure 33-center a zoom near the obstacle.

The testcase IIIb features the same geometries as in testcase IIIa, but now σ_B has a $\pm 50\%$ variation. Still both TR and PC are able to detect the location of the obstacle (Figure 14), but the recovered shape begins to suffer a distortion, because of the strong nonlinearity in the coefficient.

Analogously, in the testcases IVa and IVb the variations in σ_B are $\pm 50\%$ and $\pm 60\%$, respectively. As in the homogeneous case, the outer obstacles are well detected by both TR and PC, but only TR provides also some informations in the internal region (Figures 16,17).

The testcase V treats a linear coefficient σ_B that ranges between 4 and 18 approximately, while the testcase VI treats a radial coefficient σ_B . As before (Figures 18,19), TR and PC can accurately detect the location and the shape of the obstacle.

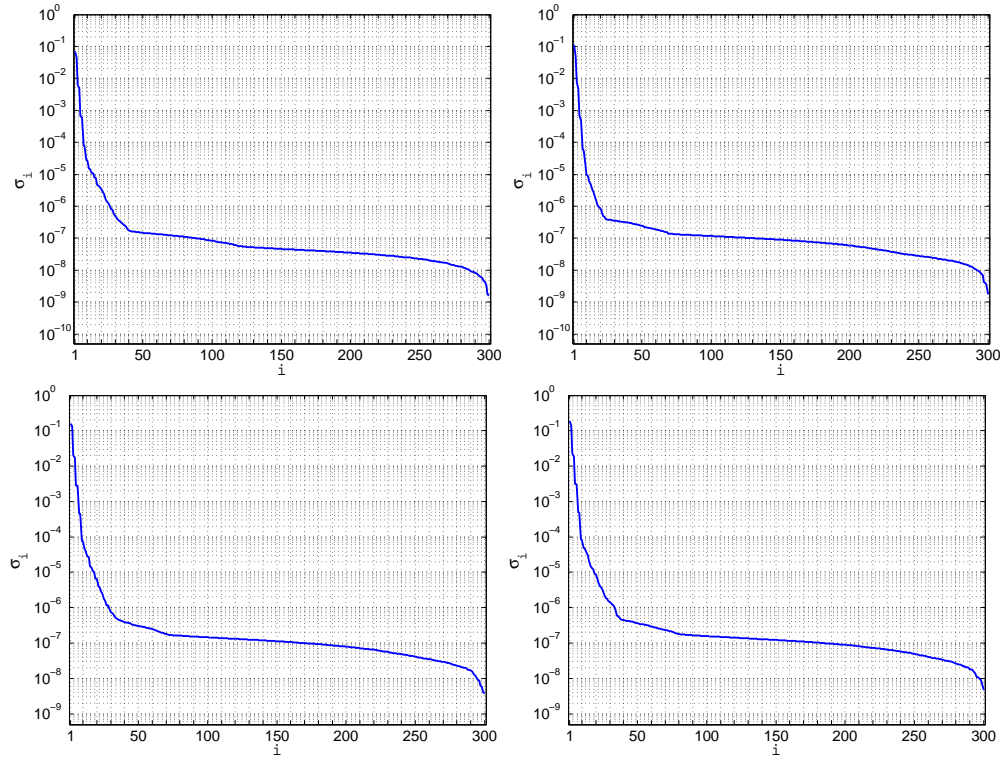


Fig. 10: Singular values σ_i of $\tilde{\Lambda}^{1/2}$. Testcase I (top-left). Testcase II (top-right). Testcase IIIa . Testcase IIIb (bottom-right).

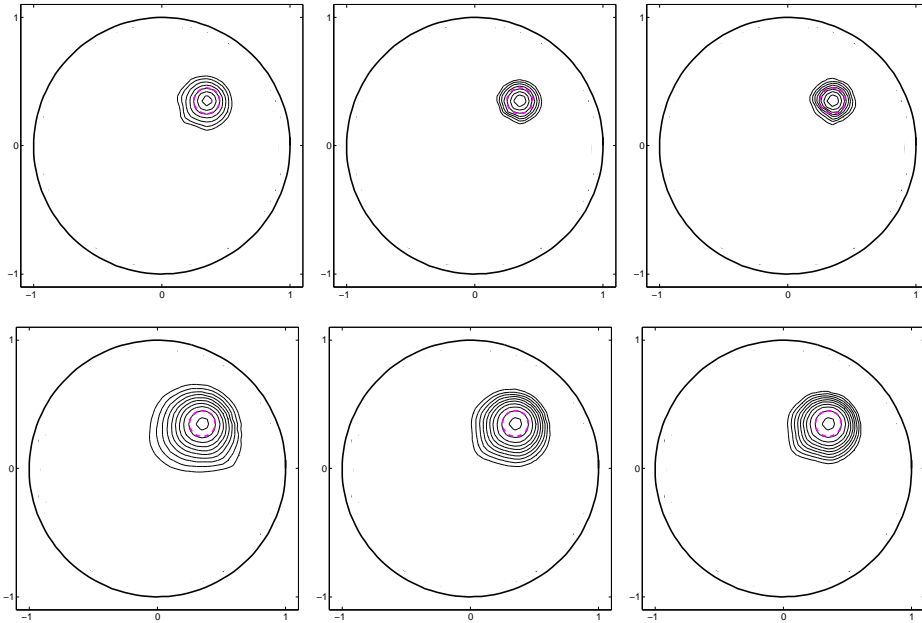


Fig. 11: Testcase I. Isolines of $C(\xi)$ in $[C_{\min}^{0.6}, C_{\max}]$. Tikhonov regularization: $\gamma = 5e - 2$ (left), $\gamma = 1e - 2$ (center), $\gamma = 5e - 3$ (right). Picard criterion, $m = 10$ (left), $m = 25$ (center), $m = 50$ (right).

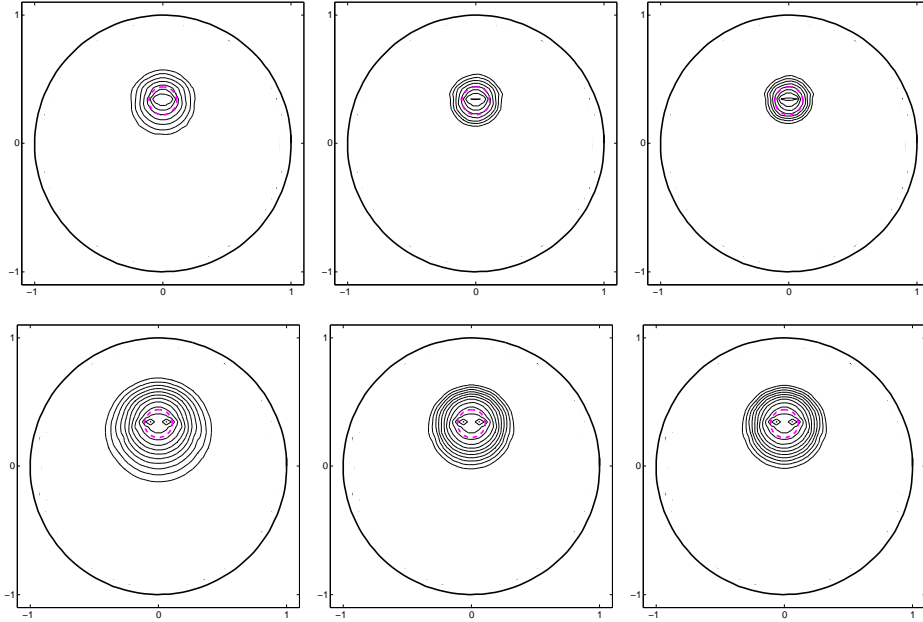


Fig. 12: Testcase II. Isolines of $C(\xi)$ in $[C_{\min}^{0.6}, C_{\max}]$. Tikhonov regularization, $\gamma = 5e - 2$ (left), $\gamma = 1e - 2$ (center), $\gamma = 5e - 3$ (right). Picard criterion, $m = 10$ (left), $m = 25$ (center), $m = 50$ (right).

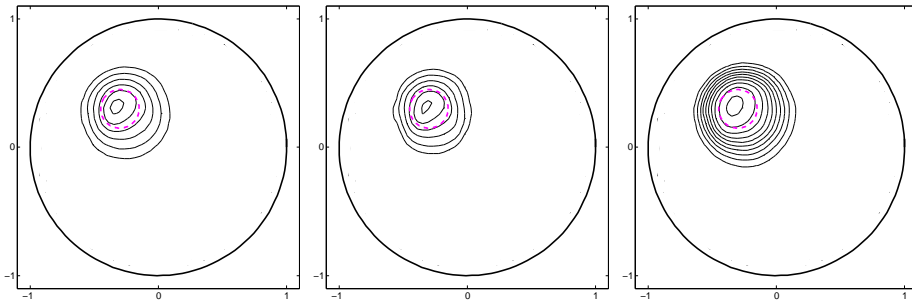


Fig. 13: Testcase IIIa. Isolines of $C(\xi)$ in $[C_{\min}^{0.5}, C_{\max}]$. Left: Tikhonov regularization, $\gamma = 1e - 1$. Center: Tikhonov regularization, $\gamma = 5e - 2$. Right: Picard criterion, $m = 25$.

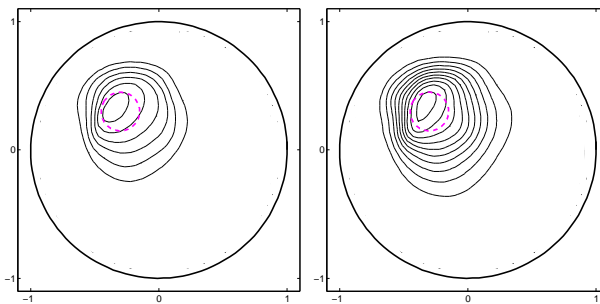


Fig. 14: Testcase IIIb. Isolines of $C(\xi)$ in $[C_{\min}^{0.5}, C_{\max}]$. Left: Tikhonov regularization, $\gamma = 5e - 1$. Right: Picard criterion, $m = 10$.

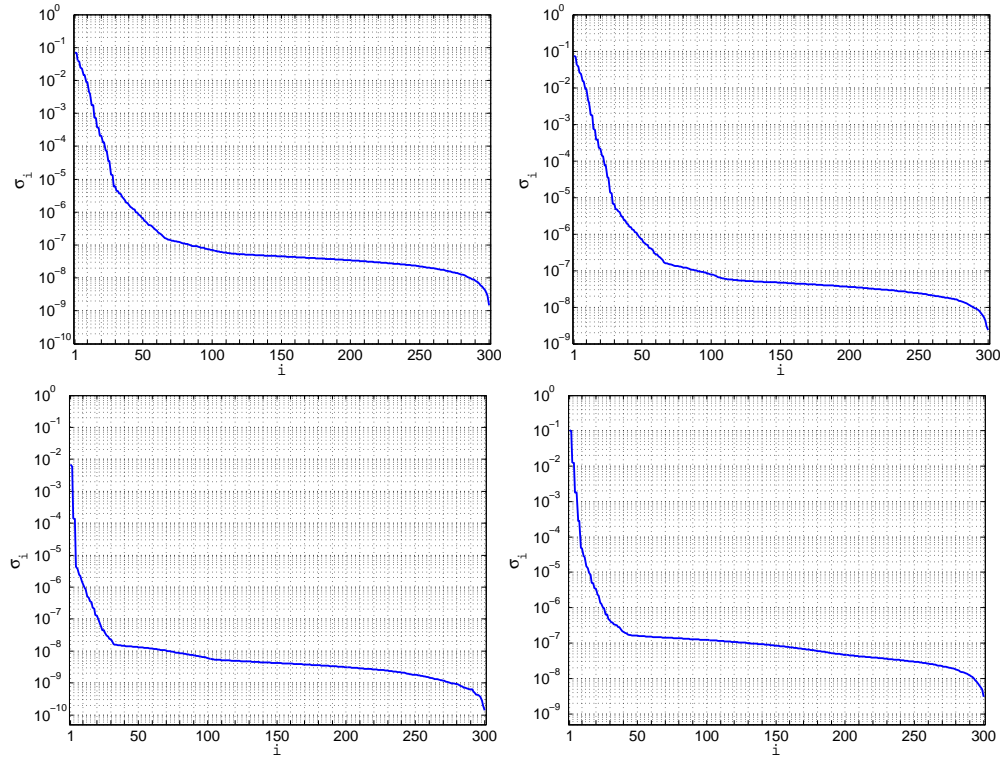


Fig. 15: Singular values σ_i of $\tilde{\Lambda}^{1/2}$. Testcase IVa (top-left). Testcase IVb (top-right). Testcase V (bottom-left). Testcase VI (bottom-right).

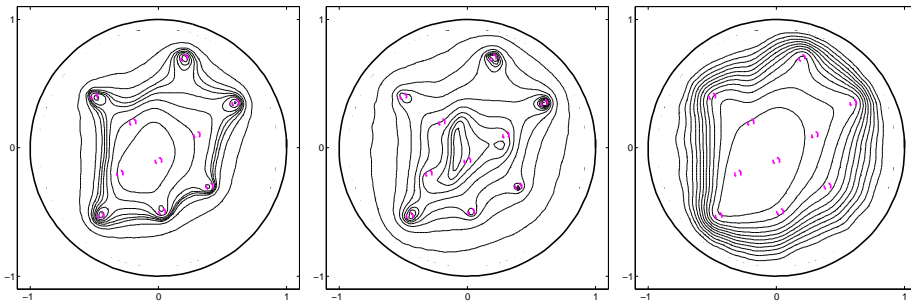


Fig. 16: Testcase IVa. Isolines of $C(\xi)$. Left: Tikhonov regularization, $\gamma = 5e-3$. Center: Tikhonov regularization, $\gamma = 1e-3$. Right: Picard criterion, $m = 25$.

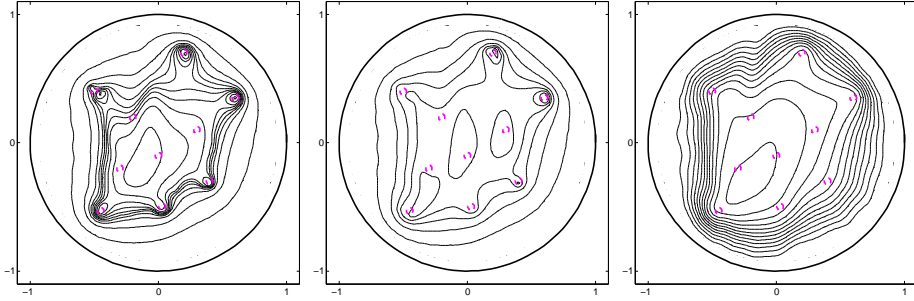


Fig. 17: Testcase IVb. Isolines of $C(\xi)$. Left: Tikhonov regularization, $\gamma = 5e - 3$. Center: Tikhonov regularization, $\gamma = 1e - 3$. Right: Picard criterion, $m = 25$.

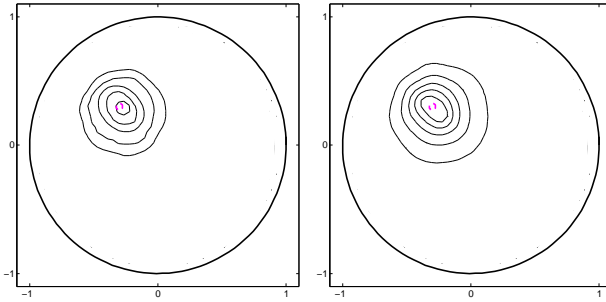


Fig. 18: Testcase V. Isolines of $C(\xi)$ in $[C_{\min}^{0.7}, C_{\max}]$. Left: Tikhonov regularization, $\gamma = 5$. Right: Picard criterion, $m = 25$.

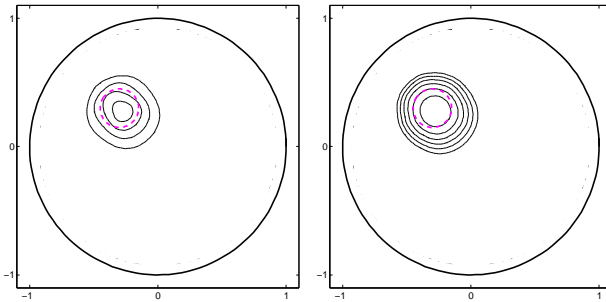


Fig. 19: Testcase VI. Isolines of $C(\xi)$ in $[C_{\min}^{0.7}, C_{\max}]$. Left: Tikhonov regularization, $\gamma = 1e - 1$. Right: Picard criterion, $m = 25$.

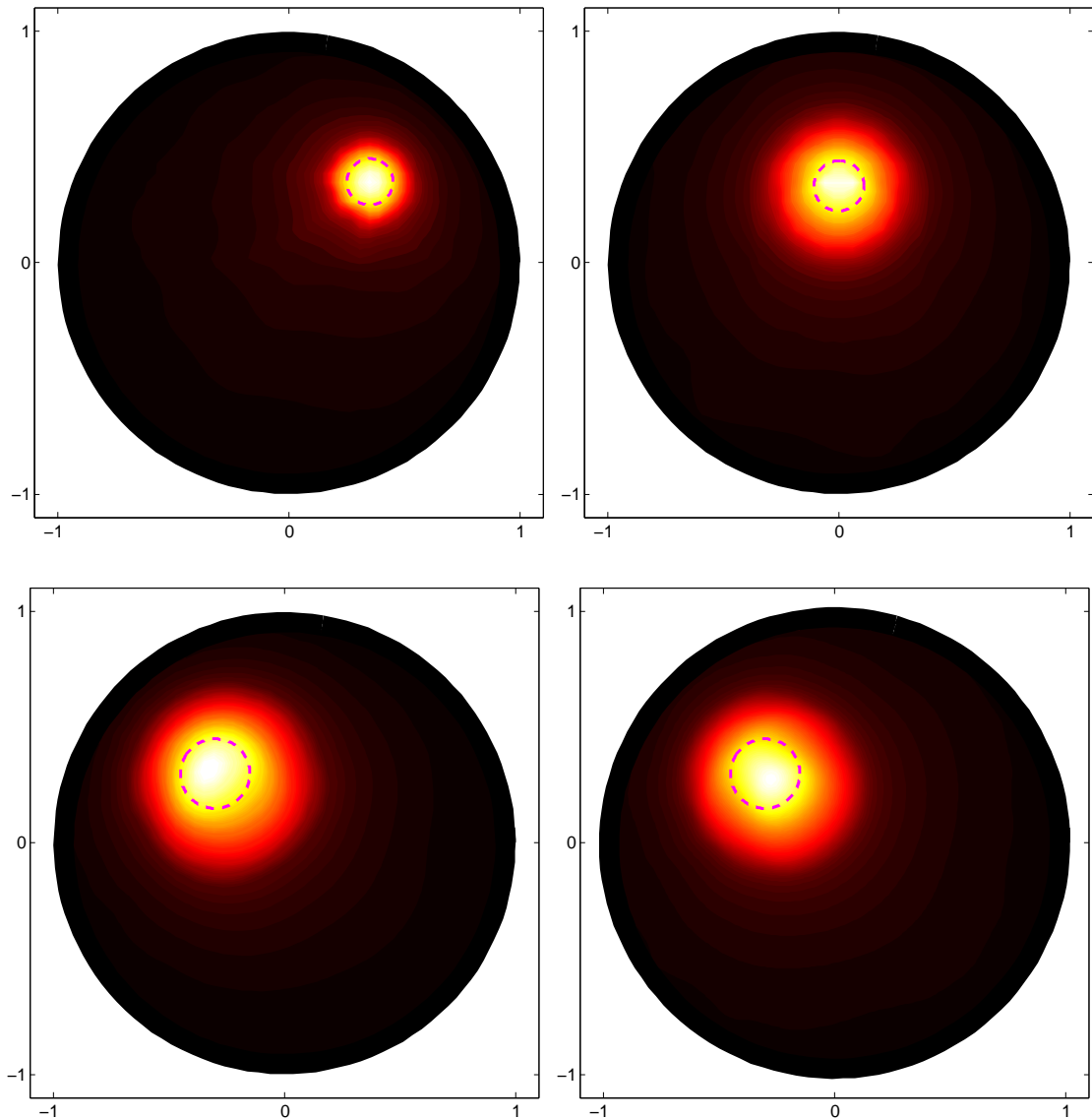


Fig. 20: Tikhonov regularization. Testcase I, $\gamma = 1e - 2$ (top-left). Testcase II, $\gamma = 5e - 2$ (top-right). Testcase IIIa, $\gamma = 1e - 1$ (bottom-left). Testcase VI, $\gamma = 1e - 2$ (bottom-right).

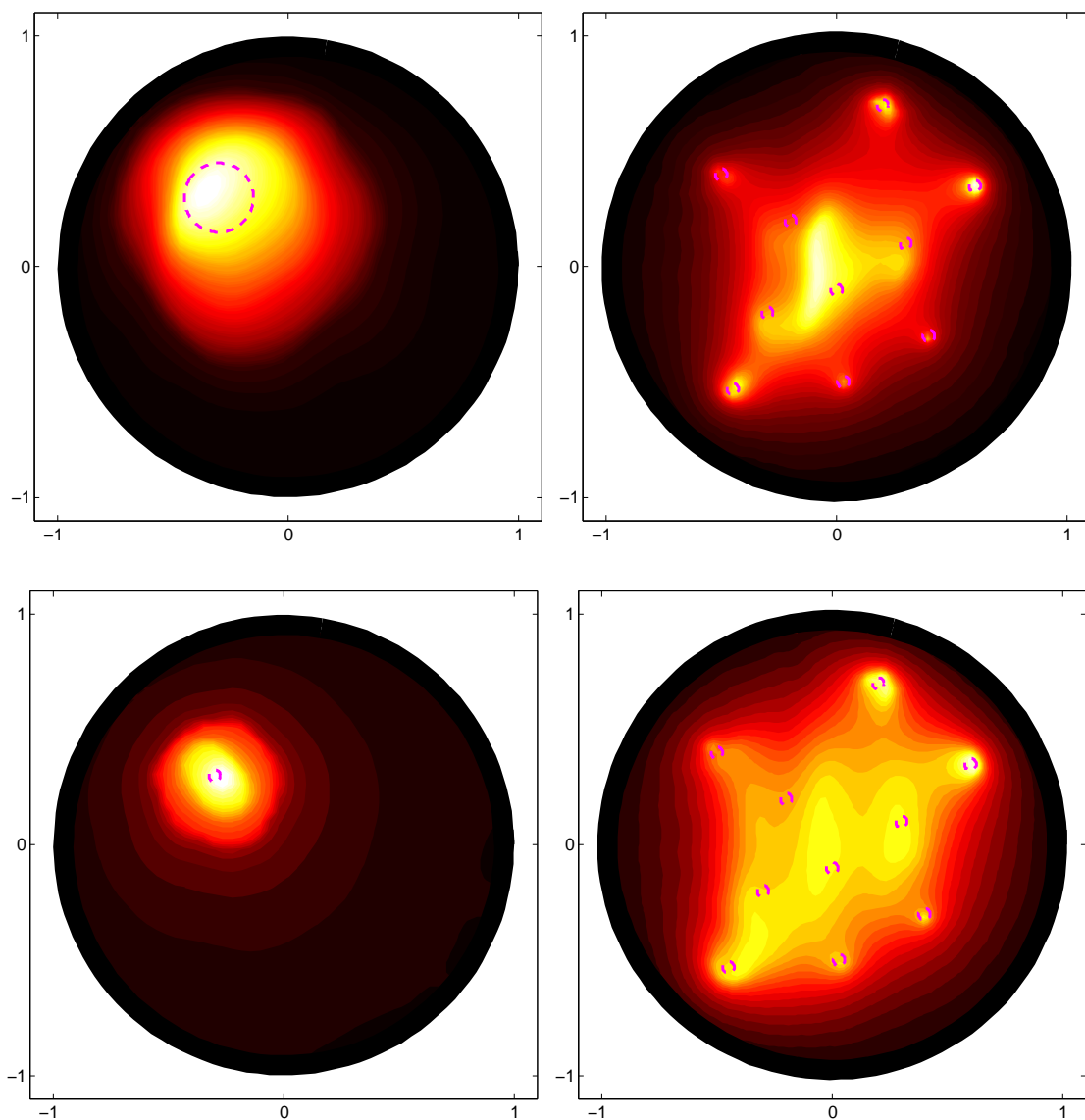


Fig. 21: Tikhonov regularization. . Testcase IIIb, $\gamma = 5e - 1$ (top-left). Testcase IVa, $\gamma = 1e - 3$ (top-right). Testcase V, $\gamma = 5$ (bottom-left). Testcase IVb, $\gamma = 1e - 3$ (bottom-right).

4.3 Measures with noise

Now we investigate the sensitivity of our results to noisy perturbations. To this aim we perturb the operator M with the random matrix U , $U_{ij} \stackrel{\text{i.i.d.}}{\sim} \mathbb{U}([-1, 1])$, scaled to the spectral norm of M :

$$M_\mu = M + \mu \|M\|_2 \frac{U}{\|U\|_2}. \quad (4.2)$$

The parameter μ represents the magnitude of the noisy perturbation, and accordingly we will tune γ in (3.5) or m in (3.8). In presence of noise the isolines obtained with TR are identical to those obtained without noise, as long as a sufficient number of the largest singular values are not obfuscated. The effect of noise is an attenuation of the values in the indicator function (4.1). This holds also for large amount of noise, up to 10%.

Figures 22, 23, 24, 25, 26, show the results obtained for the testcases A,C,II,IIIa,IVa after adding 0.1% or 1% of noise. This correspond to pick $\mu = 1e - 2$ or $\mu = 1e - 3$, respectively, in (4.2).

The indicator function (4.1) using PC is attenuated a lot faster, preventing the recoverage of the obstacle also for small amount of noise. Therefore TR should be preferred to PC in case of noisy data.

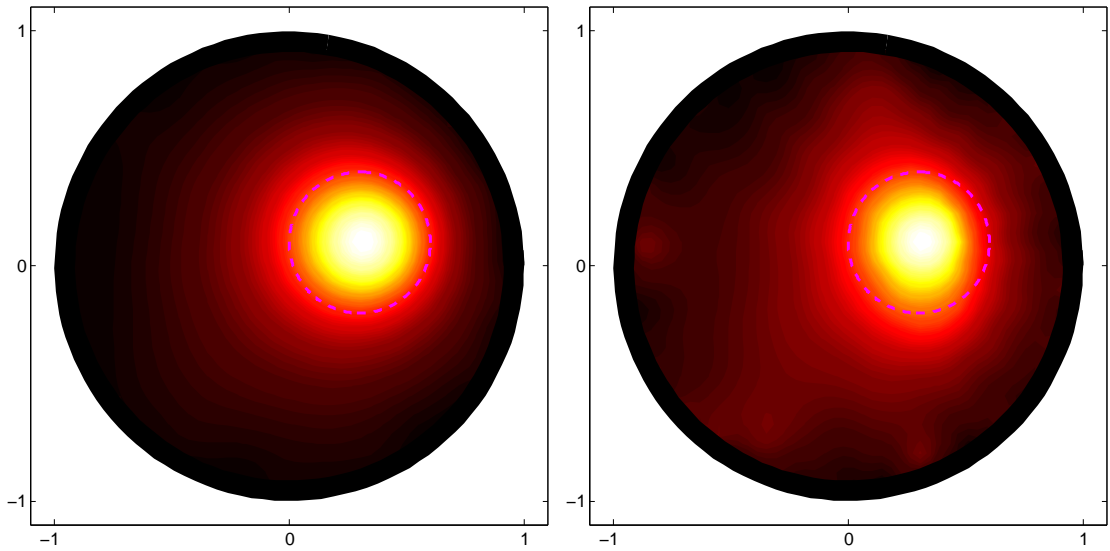


Fig. 22: Testcase A. Tikhonov regularization, $\gamma = 5e - 3$. Left: 0.1% noise. Right: 1% noise.

5 Conclusions

We proposed a numerical scheme to solve the dipole-like Neumann problem featuring an inhomogeneous coefficient. Then we applied this scheme in the Factorization Method extended to the framework of Electrical Impedance Tomography.

We showed that the method is capable of accurately recovering the location and the shape of the inclusions, in cases where the background has variations up to one order of magnitude, and in cases where the coefficient in nonlinearly space-dependent. Two types of range test are compared, one based on Tikhonov regularization and one based on the Picard criterion. The former performs more accurately, although in some cases also the latter yields a precise reconstruction. The method also proved to be robust within a reasonable range of noisy perturbations.

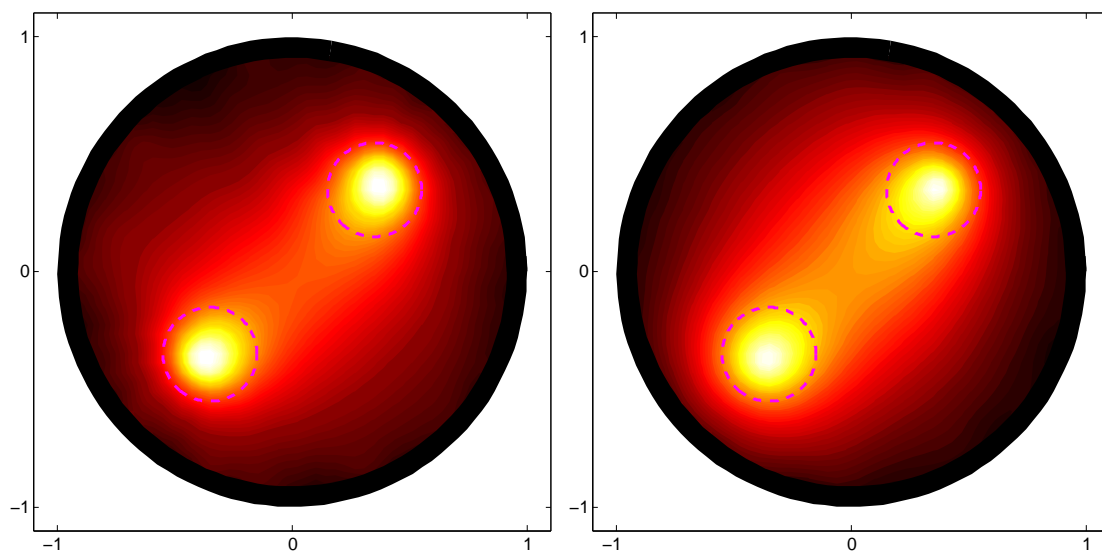


Fig. 23: Testcase C. Tikhonov regularization, $\gamma = 5e - 4$. Left: 0.1% noise. Right: 1% noise.

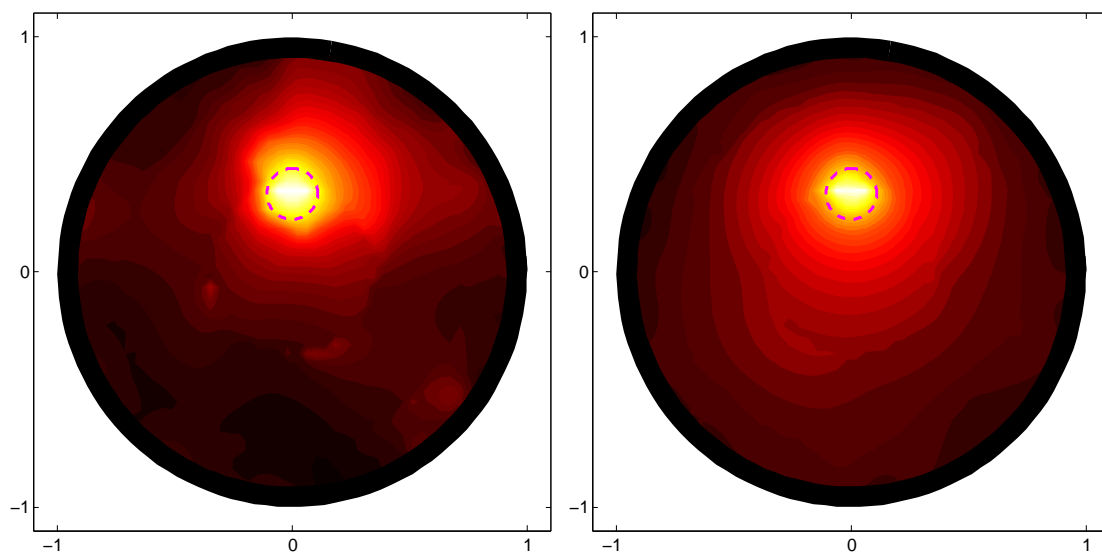


Fig. 24: Testcase II. Tikhonov regularization, $\gamma = 5e - 2$. Left: 0.1% noise. Right: 1% noise.

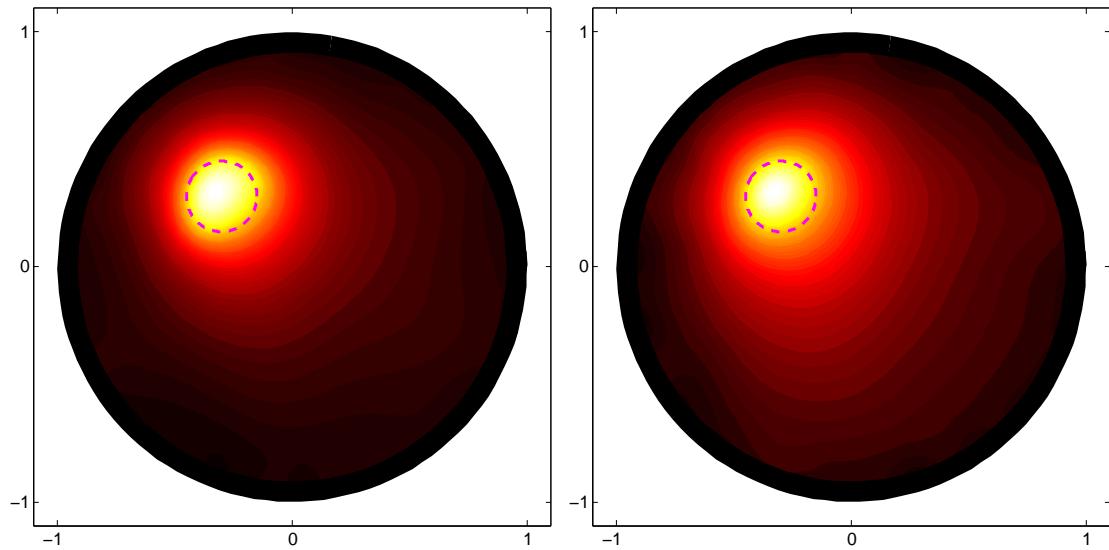


Fig. 25: Testcase IIIa. Tikhonov regularization, $\gamma = 1e - 1$. Left: 0.1% noise. Right: 1% noise.

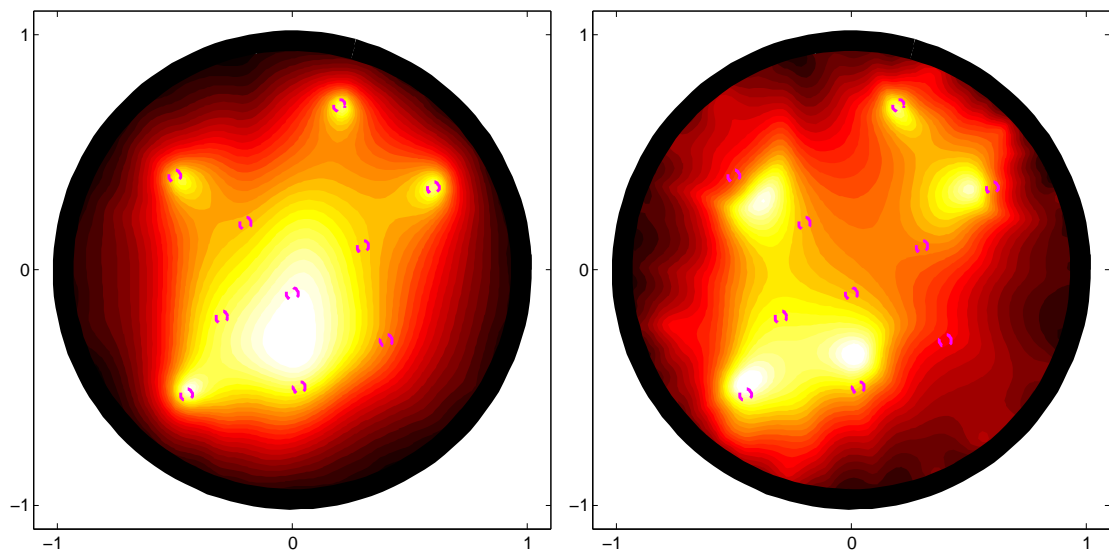


Fig. 26: Testcase IVa. Tikhonov regularization, $\gamma = 1e - 3$. Left: 0.1% noise. Right: 1% noise.

A Exact geometries

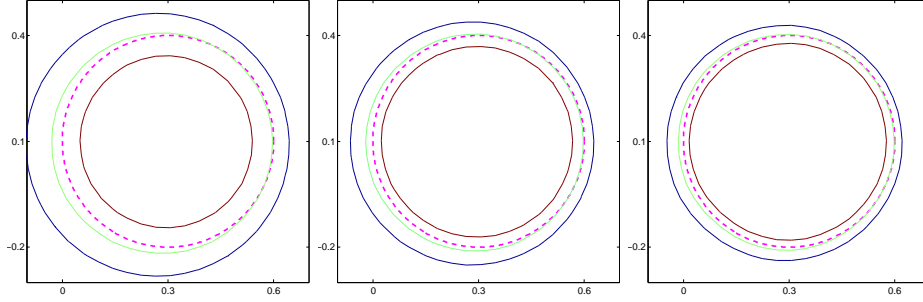


Fig. 27: Testcase A. Exact geometry (dashed purple line), isolines $C_{\min}^{0.9}$ (blue), C_{\min}^1 (green), $C_{\min}^{1.1}$ (brown). Tikhonov regularization: $\gamma = 5e - 1$ (left), $\gamma = 5e - 2$ (center), $\gamma = 5e - 3$ (right).

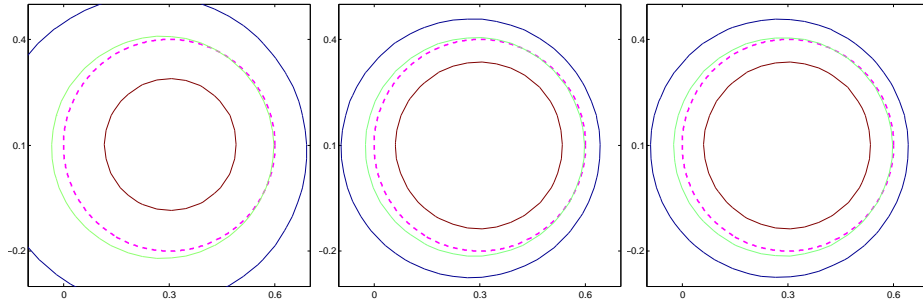


Fig. 28: Testcase A. Exact geometry (dashed purple line), isolines $C_{\min}^{0.9}$ (blue), C_{\min}^1 (green), $C_{\min}^{1.1}$ (brown). Picard criterion, $m = 5$ (left), $m = 25$ (center), $m = 50$ (right).

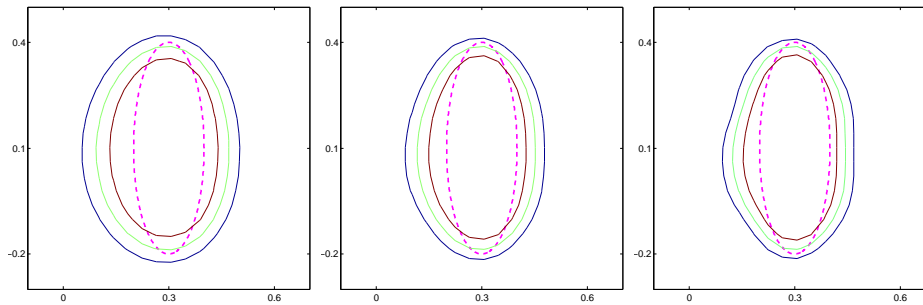


Fig. 29: Testcase D. Exact geometry (dashed purple line), isolines $C_{\min}^{0.9}$ (blue), C_{\min}^1 (green), $C_{\min}^{1.1}$ (brown). Tikhonov regularization with $\gamma = 5e - 2$ (left), $\gamma = 1e - 2$ (center), $\gamma = 5e - 3$ (left).

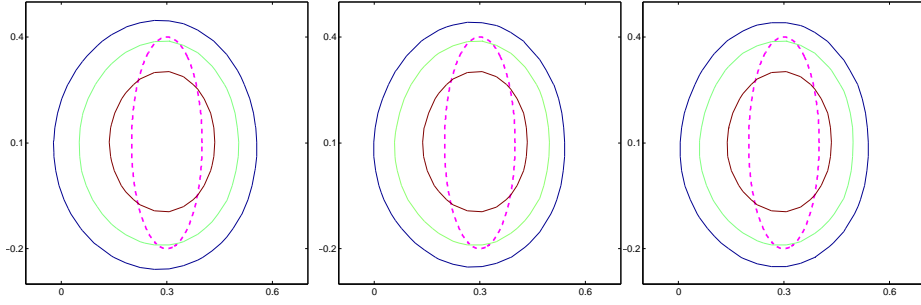


Fig. 30: Testcase D. Exact geometry (dashed purple line), isolines $C_{\min}^{0.9}$ (blue), C_{\min}^1 (green), $C_{\min}^{1.1}$ (brown). Picard criterion, $m = 10$ (left), $m = 30$ (center), $m = 50$ (right).

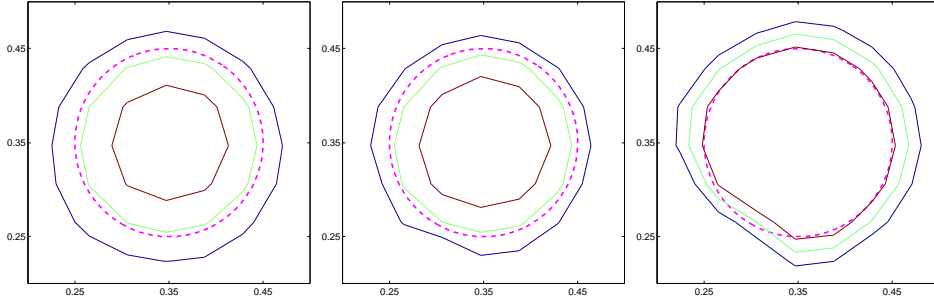


Fig. 31: Testcase I. Exact geometry (dashed purple line), isolines $C_{\min}^{0.9}$ (blue), C_{\min}^1 (green), $C_{\min}^{1.1}$ (brown). Tikhonov regularization: $\gamma = 5e - 2$ (left), $\gamma = 1e - 3$ (center), $\gamma = 5e - 3$ (right).

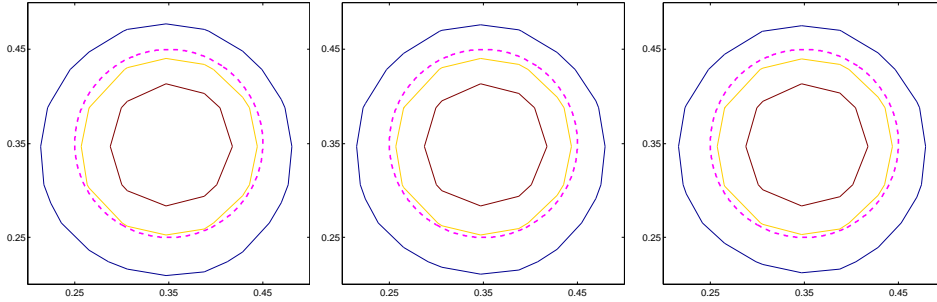


Fig. 32: Testcase I. Exact geometry (dashed purple line), isolines $C_{\min}^{0.95}$ (blue), C_{\min}^1 (orange), $C_{\min}^{1.025}$ (brown). Picard criterion, $m = 10$ (left), $m = 25$ (center), $m = 50$ (right).

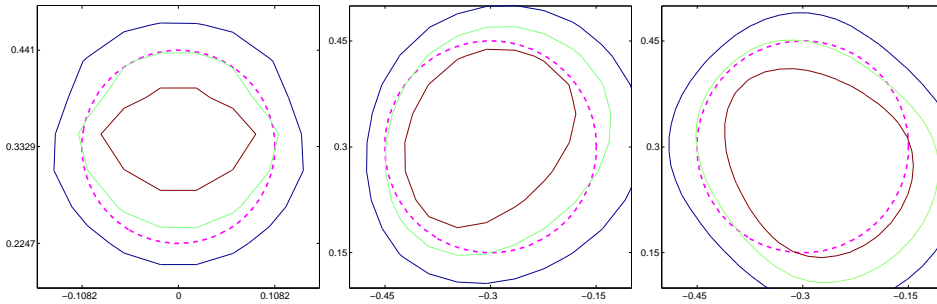


Fig. 33: Exact geometry (dashed purple line), isolines $C_{\min}^{0.9}$ (blue), C_{\min}^1 (green), $C_{\min}^{1.1}$ (brown). Testcase II, Tikhonov regularization, $\gamma = 5e - 2$. Testcase IIIa, Tikhonov regularization, $\gamma = 1e - 1$. Testcase VI, Tikhonov regularization, $\gamma = 1e - 1$.

B Well-posedness and regularity issue

We recall some regularity results for elliptic problems in the form

$$\begin{cases} -\nabla \cdot (\sigma(\mathbf{x}) \nabla u(\mathbf{x})) = f(\mathbf{x}), & \text{in } \Omega, \\ \sigma(\mathbf{x}) \nabla u(\mathbf{x}) \cdot \nu = h(\mathbf{x}), & \text{on } \partial\Omega, \end{cases} \quad (\text{B.1})$$

under the assumptions:

- Ω bounded subset of \mathbb{R}^2 ,
- $\sigma_{\min} |\xi|^2 \leq \sigma(\mathbf{x}) \xi \cdot \xi \leq \sigma_{\max} |\xi|^2$, $\forall \xi \in \mathbb{R}^2$, almost everywhere in Ω ,
- $f \in L^2(\Omega)$.

Problem (1.2) is an example of (B.1), while problem (1.5) reduces to (B.1) if the singularity in ξ is removed. The proofs of the following results can be found in [11].

Theorem 10. *Given a bounded Lipschitz domain Ω , if $f \in L^2(\Omega)$ and $g \in L^2(\partial\Omega)$ then one of the following alternatives hold:*

- *problem (B.1) has a unique solution $u \in H^1(\Omega)$ and*

$$\|u\|_{H^1(\Omega)} \leq C(\sigma_{\min}, \sigma_{\max}) \left(\|f\|_{L^2(\Omega)} + \|h\|_{L^2(\partial\Omega)} \right),$$

- *the homogeneous problem (B.1) (with $f \equiv 0$ and $h \equiv 0$) and its adjoint homogeneous problem have each the same finite number of linearly independent solutions.*

Moreover, problem (B.1) has a solution if and only if

$$\int_{\Omega} f w \, d\mathbf{x} + \int_{\partial\Omega} h w \, d\sigma = 0, \quad (\text{B.2})$$

for every solution w of the adjoint homogeneous problem associated to (B.1).

One can show that the solutions of the adjoint homogeneous problem associated to (B.1) are the constant functions. Thus from (B.2) we recover the usual compatibility condition.

Theorem 11 (H^2 interior regularity of the solution of problem (B.1)). *If the components of the coefficient $\sigma(\mathbf{x})$ are Lipschitz in Ω , then the solution $u \in H_{loc}^2(\Omega)$. Moreover, if $\Omega' \subset\subset \Omega$ then*

$$\|u\|_{H^2(\Omega')} \leq C(\sigma_{\min}, \sigma_{\max}, \text{dist}(\partial\Omega, \Omega'), K) \left(\|f\|_{L^2(\Omega)} + \|u\|_{L^2(\Omega)} \right),$$

where K is the Lipschitzian constant of $\sigma(\cdot)$.

Theorem 11 shows that u is a strong solution. Increasing the regularity of the data the solution also increases its regularity.

Theorem 12 (Global regularity of the solution of problem (B.1)). *Let Ω be a bounded C^2 -domain in \mathbb{R}^2 . If the components of the coefficient $\sigma(\mathbf{x})$ are Lipschitz in Ω and $f(\mathbf{x}) \in L^2(\Omega)$, then $u \in H^2(\Omega)$ and*

$$\|u\|_{H^2(\Omega)} \leq C \left(\|f\|_{L^2(\Omega)} + \|u\|_{L^2(\Omega)} + \|h\|_{H^{1/2}(\partial\Omega)} \right),$$

where K is the Lipschitzian constant of $\sigma(\cdot)$.

Theorem 13 (Higher global regularity of the solution of problem (B.1)). *Given $m \geq 1$, let Ω be a bounded C^{m+2} -domain in \mathbb{R}^2 . If*

$$\sigma(\mathbf{x})_{ij} \in C^{m+1}(\overline{\Omega}), \quad f(\mathbf{x}) \in H^m(\Omega) \quad \text{and} \quad h \in C^{m+1/2}(\partial\Omega),$$

then $u \in H^{m+2}(\Omega)$ and

$$\|u\|_{H^{m+2}(\Omega)} \leq C \left(\|f\|_{H^m(\Omega)} + \|u\|_{L^2(\Omega)} + \|h\|_{H^{m+1/2}(\partial\Omega)} \right).$$

From Theorem 13 we see that if Ω is a C^∞ -domain, $\sigma(\mathbf{x})_{ij} \in C^\infty(\overline{\Omega})$, $f(\mathbf{x}) \in C^\infty(\Omega)$ and $h \in C^\infty(\partial\Omega)$ then $u \in C^\infty(\overline{\Omega})$.

References

- [1] Giovanni Alessandrini. Stable determination of conductivity by boundary measurements. *Appl. Anal.*, 27(1-3):153–172, 1988.
- [2] Habib Ammari and Hyeonbae Kang. *Polarization and moment tensors*, volume 162 of *Applied Mathematical Sciences*. Springer, New York, 2007.
- [3] Kari Astala and Lassi Päiväranta. Calderón’s inverse conductivity problem in the plane. *Ann. of Math. (2)*, 163(1):265–299, 2006.
- [4] Mustapha Azzouz, Martin Hanke, Chantal Oesterlein, and Karl Schilcher. The factorization method for electrical impedance tomography data from a new planar device. *International Journal of Biomedical Imaging*, 2007.
- [5] Russell M. Brown and Rodolfo H. Torres. Uniqueness in the inverse conductivity problem for conductivities with $3/2$ derivatives in L^p , $p > 2n$. *J. Fourier Anal. Appl.*, 9(6):563–574, 2003.
- [6] Martin Brühl. Explicit characterization of inclusions in electrical impedance tomography. *SIAM J. Math. Anal.*, 32(6):1327–1341 (electronic), 2001.
- [7] Martin Brühl, Martin Hanke, and Michael S. Vogelius. A direct impedance tomography algorithm for locating small inhomogeneities. *Numer. Math.*, 93(4):635–654, 2003.
- [8] Alberto-P. Calderón. On an inverse boundary value problem. In *Seminar on Numerical Analysis and its Applications to Continuum Physics (Rio de Janeiro, 1980)*, pages 65–73. Soc. Brasil. Mat., Rio de Janeiro, 1980.
- [9] D. J. Cedio-Fengya, S. Moskow, and M. S. Vogelius. Identification of conductivity imperfections of small diameter by boundary measurements. Continuous dependence and computational reconstruction. *Inverse Problems*, 14(3):553–595, 1998.
- [10] Heinz W. Engl, Martin Hanke, and Andreas Neubauer. *Regularization of inverse problems*, volume 375 of *Mathematics and its Applications*. Kluwer Academic Publishers Group, 1996.
- [11] Lawrence C. Evans. *Partial Differential Equations*. American Mathematical Society, 1997.
- [12] Bastian Gebauer and Nuutti Hyvönen. Factorization method and irregular inclusions in electrical impedance tomography. *Inverse Problems*, 23(5):2159–2170, 2007.
- [13] Martin Hanke and Birgit Schappel. The factorization method for electrical impedance tomography in the half-space. *SIAM J. Appl. Math.*, 68(4):907–924, 2008.

-
- [14] Andreas Kirsch and Natalia Grinberg. *The factorization method for inverse problems*. Oxford University Press, 2008.
 - [15] Armin Lechleiter, Nuutti Hyvönen, and Harri Hakula. The factorization method applied to the complete electrode model of impedance tomography. *SIAM J. Appl. Math.*, 68(4):1097–1121, 2008.
 - [16] John M. Lee and Gunther Uhlmann. Determining anisotropic real-analytic conductivities by boundary measurements. *Comm. Pure Appl. Math.*, 42(8):1097–1112, 1989.
 - [17] O. Scherzer, editor. *Handbook of Mathematical methods in Imaging*. Springer, 2010.
 - [18] Y Zou and Z Guo. A review of electrical impedance techniques for breast cancer detection. *Medical Engineering & Physics*, 25(2):79 – 90, 2003.



Centre de recherche INRIA Saclay – Île-de-France
Parc Orsay Université - ZAC des Vignes
4, rue Jacques Monod - 91893 Orsay Cedex (France)

Centre de recherche INRIA Bordeaux – Sud Ouest : Domaine Universitaire - 351, cours de la Libération - 33405 Talence Cedex
Centre de recherche INRIA Grenoble – Rhône-Alpes : 655, avenue de l'Europe - 38334 Montbonnot Saint-Ismier
Centre de recherche INRIA Lille – Nord Europe : Parc Scientifique de la Haute Borne - 40, avenue Halley - 59650 Villeneuve d'Ascq
Centre de recherche INRIA Nancy – Grand Est : LORIA, Technopôle de Nancy-Brabois - Campus scientifique
615, rue du Jardin Botanique - BP 101 - 54602 Villers-lès-Nancy Cedex
Centre de recherche INRIA Paris – Rocquencourt : Domaine de Voluceau - Rocquencourt - BP 105 - 78153 Le Chesnay Cedex
Centre de recherche INRIA Rennes – Bretagne Atlantique : IRISA, Campus universitaire de Beaulieu - 35042 Rennes Cedex
Centre de recherche INRIA Sophia Antipolis – Méditerranée : 2004, route des Lucioles - BP 93 - 06902 Sophia Antipolis Cedex

Éditeur
INRIA - Domaine de Voluceau - Rocquencourt, BP 105 - 78153 Le Chesnay Cedex (France)
<http://www.inria.fr>
ISSN 0249-6399